

MARTIN MARIETTA ENERGY SYSTEMS LIBRARIES



3 4456 0069229 4

ORNL/TM-9648

ornl

**OAK RIDGE
NATIONAL
LABORATORY**

MARTIN MARIETTA

Determination of High-Temperature Fluid Viscosity Using Dynamic Light Scattering

D. F. Williams
C. H. Byers
J. S. Watson

OAK RIDGE NATIONAL LABORATORY
CENTRAL RESEARCH LIBRARY
CIRCULATION SECTION
SUITE ROOM 175
LIBRARY LOAN COPY
DO NOT TRANSFER TO ANOTHER PERSON
If you wish someone else to use this
report, send in name with report and
the library will arrange a loan.

OPERATED BY
MARTIN MARIETTA ENERGY SYSTEMS, INC.
FOR THE UNITED STATES
DEPARTMENT OF ENERGY

Printed in the United States of America. Available from
National Technical Information Service
U.S. Department of Commerce
5285 Port Royal Road, Springfield, Virginia 22161
NTIS price codes—Printed Copy: A06 Microfiche: A01

This report was prepared as an account of work sponsored by an agency of the United States Government. Neither the United States Government nor any agency thereof, nor any of their employees, makes any warranty, express or implied, or assumes any legal liability or responsibility for the accuracy, completeness, or usefulness of any information, apparatus, product, or process disclosed, or represents that its use would not infringe privately owned rights. Reference herein to any specific commercial product, process, or service by trade name, trademark, manufacturer, or otherwise, does not necessarily constitute or imply its endorsement, recommendation, or favoring by the United States Government or any agency thereof. The views and opinions of authors expressed herein do not necessarily state or reflect those of the United States Government or any agency thereof.

Chemical Technology Division

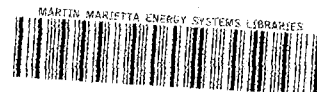
DETERMINATION OF HIGH-TEMPERATURE FLUID VISCOSITY
USING DYNAMIC LIGHT SCATTERING

D. F. Williams
C. H. Byers
J. S. Watson

This report was prepared as a thesis and submitted to the Faculty of the Graduate School of the University of Tennessee in partial fulfillment of the degree of Master of Science in the Department of Chemical Engineering.

Date Published - August 1986

Prepared by
OAK RIDGE NATIONAL LABORATORY
Oak Ridge, Tennessee 37831
operated by
MARTIN MARIETTA ENERGY SYSTEMS, INC.
for the
U. S. DEPARTMENT OF ENERGY
under Contract No. DE-AC05-84OR21400



3 4456 0069229 4

ACKNOWLEDGMENTS

I would like to first thank my associate, Mr. Ron Brunson, for his assistance in performing the experiments described in this report. His diligence and care, along with his positive attitude, helped make this work possible. The interest of Dr. John F. Fellers and Dr. Joseph J. Perona stimulated progress in my work. The interest and support of Dr. Mark C. Wittels of the Department of Energy Office of Basic Energy Sciences are also greatly appreciated. Ms. Mary Ann Neal and Ms. Brenda Breeden should be commended for their patience and diligence in typing and correcting this manuscript. Finally, the support of many of my colleagues at Oak Ridge National Laboratory was indeed invaluable.

ABSTRACT

The measurement and prediction of liquid-phase transport properties are of both fundamental and applied interest. In particular, the measurement and prediction of high-temperature-liquid viscosities pose some important problems. Conventional measurement techniques do not readily apply to systems far above the normal boiling point. At temperatures below the normal boiling point, measurements can be correlated accurately in an empirical form; at higher temperatures, however, a need exists for more high-quality data and more accurate predictive methods.

A light-scattering method for measurement of high-temperature viscosities was developed in this study. Dynamic light scattering was used to measure viscosity by characterizing the effect of fluid drag on the motion of suspended microparticles. The critical experimental factors were identified and analyzed. Stabilization of the model microparticles against aggregation was found to be of prime importance, and this topic is discussed in detail. Selected predictive correlations for viscosity were also examined and evaluated.

Experimental measurements were made on a group of aliphatic and cyclic organic compounds. Cyclohexane, n-pentane, n-heptane, toluene, and chloroform were investigated at temperatures as high as 90% of the critical temperature. Both an ideal mixture (n-pentane/n-heptane) and an interacting mixture (n-hexane/isopropanol) were examined at elevated temperatures in order to study behavioral characteristics. Results were found to be consistent with the best literature data. Only the corresponding-states methods offered any true predictive validity. At high temperatures ($T_r > 0.70$), these methods exhibited good accuracy.

TABLE OF CONTENTS

Section	Page
INTRODUCTION	1
I. THEORETICAL BACKGROUND	5
Viscosity	5
Light Scattering	13
Brownian motion theory	13
Light-scattering theory	16
Recent studies	26
II. EXPERIMENTAL	29
Strategy-Seed Particles and Colloidal Stability	29
Apparatus	32
Materials and Procedures	40
Preparation of organophilic sols	40
Light-scattering measurements	42
III. DISCUSSION OF RESULTS	45
Pure Components	45
Mixtures	60
IV. CONCLUSIONS	65
LIST OF REFERENCES	67
APPENDIXES	73
Appendix A. TABULATION OF EXPERIMENTAL DATA DETERMINED BY LIGHT SCATTERING	75
Appendix B. VISCOSITY ESTIMATION METHOD OF LEE	81
Appendix C. ESTIMATION OF REFRACTIVE INDEX	85
Appendix D. COMPUTER PROGRAM DOCUMENTATION	89

LIST OF TABLES

Table	Page
1. Standard particle diameters (at 20°C) by light-scattering before and after high-temperature operation	46
2. Typical viscosity measurements during corresponding heating and cooling cycles (Sample No. 3.146; Solvent = n-pentane).	47
3. Comparison of viscosity data and recommended correlations . . .	53
4. Lee's triple-point parameter (ϵ): fitted, estimated, and calculated literature values.	60

LIST OF FIGURES

Figure	Page
1. Typical behavior of the autocorrelation function (A^*) of a periodic signal (A)	18
2. Typical results from a dynamic light-scattering experiment .	21
3. Dynamic light-scattering spectrometer for high-temperature experiments	33
4. Operation of the high-temperature spectrometer.	34
5. High-temperature, high-pressure enclosure diagram (heater channels not shown)	36
6. Photograph of high-temperature, high-pressure enclosure explosion view	37
7. High-temperature, high-pressure enclosure — top view during operation	38
8. Viscosity of <u>n</u> -pentane: experimental results, literature values, and predictions	48
9. Viscosity of <u>n</u> -heptane: experimental results, literature values, and predictions	49
10. Viscosity of cyclohexane: experimental results and predictions	50
11. Viscosity of chloroform: experimental results and predictions	51
12. Viscosity of toluene: experimental results and predictions .	52
13. Comparison of viscosity data and Lee predictions for <u>n</u> -pentane	56

Figure	Page
14. Comparison of viscosity data and Lee predictions for <u>n</u> -heptane	57
15. Comparison of viscosity data and Lee predictions for cyclohexane	58
16. Comparison of viscosity data and Lee predictions for toluene	59
17. Mixture viscosity data and predictions for <u>n</u> -pentane/ <u>n</u> -heptane binary (50-50 mol %)	61
18. Mixture viscosity data and predictions for nonideal binary system (75.7 mol % n-hexane, 24.3 mol % isopropanol) . . .	63

NOMENCLATURE

- $A(t)$ - arbitrary signal, continuous function of time
 A_j - arbitrary signal, discrete function of time
 $\bar{A}(t)$ - fluctuating influence of molecular collisions on particle motion
 $A^*(\tau)$ - time-domain autocorrelation function of $A(t)$ (heterodyne)
 ${}^2A^*(\tau)$ - same as $A^*(\tau)$, except applies to homodyne condition
 $A^*(\omega)$ - frequency-domain scattering results
 D - self-diffusion coefficient = $kT/(6\pi a\eta)$
 $E(t)$ - electric field amplitude
 $E_s(t)$ - scattered electric field
 $G(\Gamma)$ - normalized distribution of scattering line widths
 K - arbitrary constant
 M - molecular weight
 P - pressure
 $P(q,r)$ - Mie scattering factor
 $P(\bar{u}_0)$ - probability of occurrence of velocity \bar{u}_0
 R - universal gas constant
 T - temperature (absolute)
 V - specific volume
 $W(x,y;z)$ - probability of occurrence of x and y , given z
 Z - gas compressibility factor

- a - particle radius
 d_p - particle diameter
 $i = \sqrt{-1}$
 k - Boltzmann's constant
 m - particle mass
 n - medium refractive index
 \bar{q} - scattered field vector = vector difference between
 incident and scattered propagation vectors
 \bar{r} - position vector; t - time; \bar{u} - velocity vector
 x - mol fraction

 α - association parameter
 β - coefficient of dynamic friction $\sim (6\pi a\eta)/m$
 ϵ - Lee triple-point expansion parameter or corresponding-states
 energy parameter
 Γ - line width (Hz), half-width at half-height of frequency-
 domain autocorrelation function $\sim q^2 D$ (heterodyne case)
 or $\sim 2q^2 D$ (homodyne)
 η - shear viscosity
 θ - scattering angle
 λ - wavelength of light
 μ - dipole moment
 μ_n - moment of distribution, order n
 ξ - reduced viscosity parameter [Eq. (7)]
 ρ - density (molar)
 σ - corresponding-states distance parameter

τ_c - characteristic decay time of autocorrelation function

ϕ - binary interaction coefficient

ω - acentric factor or frequency

ω_s - shape factor

Subscripts

c - critical condition

i - incident condition or compound index

j - summation index, over jth condition, interval particle,
or compound

o - initial or original condition

r - reduced variable (by critical constant)

s - scattered condition

M - mixture property

INTRODUCTION

New energy and processing technologies often involve conditions of extreme temperature and pressure. The physical properties data base to support these new processes is generally sparse. Coal conversion typifies such developing areas.^{1,2} Coal conversion involves both extreme conditions ($T > 500^{\circ}\text{C}$, $P > 2000$ psia) and novel chemistry (involving complex aromatic and heterocyclic compounds). Since the necessary design data are often lacking, the development of reliable properties estimation techniques is also important. Research focusing on properties measurement and estimation is an important design input and leads to a better understanding of the process.

The primary objective of this study is to develop a new method of determining liquid viscosities at elevated temperatures. A review of viscosity measurement techniques revealed that standard viscometers (rotational, capillary, etc.) become increasingly impractical and inaccurate at high temperatures and pressures.³ In fact, relatively few compounds have been investigated in the region between the normal boiling point and the critical point. If the fluid to be studied is toxic or otherwise dangerous, this increases the difficulties in working with a conventional apparatus. Small sample volumes that are safely and easily contained within a high-pressure enclosure are more conducive to accurate measurement.

In this regard, light-scattering methods offer some distinct advantages. Since optical methods are basically nonintrusive, they are well suited to high-temperature work. The measurement cell can be kept simple, while the optical instrumentation remains physically separate

from the cell. The decoupling of the instrumentation from the high-temperature environment is a major advantage when performing experiments at extreme temperatures.

The idea of using light scattering to measure viscosity is not altogether new. Dynamic light scattering has been used to measure viscosity in some unique situations where conventional techniques were not applicable.^{4,5} However, its application to high-temperature measurements is a new development.

A perfectly homogeneous sample will not scatter light. Scattered light is a direct consequence of inhomogeneity in a liquid. Suspended colloids are a source of scattering, since the refractive index of the particle is generally different from that of the suspending liquid. The intensity of light scattered from a suspension of colloids will vary rapidly as a result of the relative motion of the microparticles.

Dynamic light scattering is used to characterize viscosity by detecting the effect of fluid drag on the motion of microparticles suspended in a fluid. As the particles diffuse in a Brownian manner, they scatter light in a way that reveals their mobility. Particle mobility is primarily a function of particle size and fluid viscosity. If the particle size is known, then one can relate the viscosity directly to the mobility parameter. This process is essentially the inverse of the particle sizing measurement that has become so popular in microbiology, polymer science, and colloid science.^{6,7}

Experimental determination of the viscosity of some important model fluids was undertaken. A group of aliphatic and cyclic hydrocarbons was examined. In particular, n-pentane, n-heptane, cyclohexane, chloroform,

and toluene were investigated from temperatures ranging from ambient to those approaching the critical point ($0.9 T_C$). The behavior of ideal (n-pentane/n-heptane) and nonideal (n-hexane/isopropanol) mixtures was also examined at normal and elevated temperatures. These data have been critically examined and evaluated with respect to the best literature data and viscosity correlations.

I. THEORETICAL BACKGROUND

Viscosity

The ability to predict liquid-phase transport properties is hampered by the lack of a broadly applicable theory of the liquid state.^{8,9} A model for liquid viscosity behavior that is as successful as that used for gases (kinetic theory, Chapman-Enskog theory) has not been developed. This lack of modeling success is primarily due to the complicated state of aggregation that exists in liquids. Gases and solids are amenable to much simpler modeling. Momentum transfer in a gas is simplified due to the large distances between individual molecules. Complex interatomic forces are not the controlling factors, as they are in liquids. Solids are more easily modeled because of their structure, which allows better characterization of the forces involved. The liquid state bridges the extremes between highly ordered and very random states of matter.

Compromise theories that view liquids as disordered solids or very dense gases have had only limited success.^{8,9} Excluded volume theories, recently popularized by Hildebrand,¹⁰ are conceptually appealing and reasonably accurate. However, predictions depend on precise volumetric data, which are generally not available. The only methods that seem to offer widespread predictive validity are those based on the theory of corresponding states.

Van der Waals initially proposed (1880s) the basic principles of the theory of corresponding states. Numerous elaborations and modifications have followed.¹¹ In its simplest form, the macroscopic theory proposes that all pure substances obey the same equation of state in terms of reduced-state variables:

$$Z = PV/RT = f(P_r, T_r) \text{ or } f(V_r, T_r) , \quad (1)$$

where

$$P_r = P/P_c,$$

$$T_r = T/T_c,$$

$$V_r = V/V_c,$$

and subscript c refers to the property at the critical point.

More recent investigators¹² have developed a microscopic (or molecular) theory of corresponding states whose basic tenets are that (1) the force between two molecules depends primarily on the distance of separation and (2) the force between two molecules is proportional to a universal function (i.e., Lennard-Jones) of their separation distance. These assumptions are strictly observed only for nonpolar molecules that exhibit spherical symmetry (i.e., noble gases, methane). This more basic view of the corresponding-states theory led to applications beyond P-V-T work.

Dimensionless analysis arguments were used to extend the application of the theory to include the estimation of transport properties.¹¹ It is presumed that the properties of the molecules can be defined by their mass (m), a characteristic distance (σ), and a characteristic energy (ϵ). The viscosity then depends on six parameters: V (volume), T (temperature), k (Boltzmann constant), m , σ , and ϵ . The reduction of variables by dimensionless analysis yields three independent dimensionless variables:

$$T^* = kT/\epsilon , \quad V^* = V/\sigma^3 , \quad \eta^* = \eta\sigma^2/\sqrt{m\epsilon} . \quad (2)$$

Therefore,

$$\eta = f(V^*, T^*) . \quad (3)$$

Subsequent analysis has put the application of the corresponding-states theory to transport properties on firm theoretical ground. Rigorous treatment of liquid-phase transport properties is based on the Louisville equation.¹¹ Statistical mechanical treatments yield equations for the shear viscosity which cannot be solved in a precise manner for real liquids;^{8,11} however, these "formal" solutions have provided validation of the two-parameter theory of corresponding states [Eq. (3)]. Mori¹³ utilized fluctuation-dissipation theory to formulate an expression for the shear viscosity as a function of the autocorrelation function of the stress tensor (S_{xy}):

$$\eta = \frac{1}{V k T} \int_0^{\tau} \langle S_{xy}(t, r) S_{xy}(0, r) \rangle dt . \quad (4)$$

Helfand and Rice¹⁴ showed that this expression for η is a function of only T^* and V^* once the equation is converted to dimensionless form. Rice and Kirkwood¹⁵ have also provided support for the two-parameter theory in their statistical mechanical formulation.

Application of corresponding-states principles to complex fluids has required the use of higher-order models to obtain good correlation. The typical form for viscosity correlation is similar to that used in P-V-T work;¹⁶

$$\eta_r = \eta/\eta_c = f(T_r, P_r \text{ or } V_r, \omega) , \quad (5)$$

where a third parameter (ω), the acentric factor, is added to explain the differences between the nonsphericity and the polarity of the compounds. The basic microscopic model does not take into account the nonsphericity,

polarity, or associative nature of the molecules. Third- and higher-order parameters are essentially empirical factors that have been devised to characterize the deviation from the assumptions of the two-parameter model.

Letsou and Stiel^{17,18} have developed a very successful correlation for predicting saturated liquid viscosities at high temperatures ($T_R > 0.7$). Only the critical constants (T_C and P_C) and the acentric factor (ω) need to be determined. According to Letsou and Stiel:

$$\eta\xi = f_1(T_R) + \omega \cdot f_2(T_R) , \quad (6)$$

where

$$\xi = (T_C)^{1/6} / \sqrt{M} \cdot P_C^{2/3} , \quad (7)$$

M = molecular weight ,

and

$$f_1 = 0.015174 - 0.02135 T_R + 0.0075 T_R^2 , \quad (8)$$

$$f_2 = 0.042522 - 0.07674 T_R + 0.0340 T_R^2 . \quad (9)$$

This correlation was developed using data for relatively nonpolar compounds. Good estimates (errors of 10%) can be calculated for compounds of low polarity. More complex correlations are needed for highly polar compounds such as water or ammonia.

Recently, a corresponding-states correlation has been developed to predict viscosities over the entire liquid temperature range (freezing point to critical point). Lee⁹ has proposed a method that utilizes triple-point properties in addition to critical parameters. The volume expansion factor at the triple point is employed to estimate molecular

orientation effects in the low-temperature regime. The basic form of the correlation is

$$(\eta - \eta^*) \cdot \gamma \cdot 10^5 = \exp(2.933 g^a + 4.542 g^b) - 1 , \quad (10)$$

$$a = 8.336 ,$$

$$b = 0.9228 ,$$

where η is the saturated liquid viscosity, η^* is the corresponding dilute gas viscosity, and γ and g are complicated functions of the triple-point properties (see Appendix B). Accuracies of >5% are claimed for nonpolar compounds over a wide temperature range.

Efforts regarding mixture viscosity prediction are not very far advanced. Many existing empirical correlations do not have any real predictive validity or broad applicability. Again, corresponding-states methods seem to offer the most promise. Teja and Rice¹⁹ suggest an approach using pseudocritical parameters (T_M , P_M , ω_M , V_M) based on the van der Waals one-fluid model:

$$T_M = \text{critical temperature of mixture} = \frac{\sum_i \sum_j x_i x_j T_{c_{ij}} V_{c_{ij}}}{\sum_i \sum_j x_i x_j V_{c_{ij}}}, \quad (11)$$

$$V_M = \text{critical volume of mixture} = \sum_i \sum_j x_i x_j V_{c_{ij}}, \quad (12)$$

$$\omega_M = \text{acentric factor of mixture} = \sum_i x_i \omega_i, \quad (13)$$

$$P_M = \text{critical pressure of mixture} = (0.2905 - 0.085 \omega_M) RT_M/V_M, \quad (14)$$

where x is mol fraction, ii and jj subscripts refer to pure components, and ij ($i \neq j$) subscript refers to the cross parameter terms defined by:

$$T_{c_{ij}} V_{c_{ij}} = \Psi_{ij} (T_{c_{ii}} x_{c_{ii}} T_{c_{jj}} x_{c_{jj}})^{1/2}, \quad (15)$$

$$V_{c_{ij}} = 1/8 (V_{c_{ii}}^{1/3} + V_{c_{jj}}^{1/3})^3. \quad (16)$$

The Ψ_{ij} coefficient is an empirically determined interaction coefficient. For ideal mixtures, $\Psi_{ij} = 1$. The resulting pseudocritical parameters are used in a corresponding-states expansion:¹⁹

$$\ln(\eta\xi)_M = \ln(\eta\xi)_1 + \frac{\omega_M - \omega_1}{\omega_2 - \omega_1} [\ln(\eta\xi)_2 - \ln(\eta\xi)_1], \quad (17)$$

where 1 and 2 refer to pure component values, M refers to pseudocritical (mixture) values, and $(\eta\xi)$ is determined by the corresponding-states correlation for the pure component. This method has provided good estimates ($\pm 2\%$) of mixture viscosity for a wide variety of compounds.

Kendall and Monroe²⁰ proposed a useful empirical predictive method for ideal mixtures. Their study led to the following equation:

$$\eta_M^{1/3} = \sum_i (x_i \eta_i^{1/3}) \quad (\text{ideal mixtures}). \quad (18)$$

This rule was adopted by the authors of API's Technical Data Book²¹ for the blending of hydrocarbons. Mixture viscosities calculated in this manner should provide good estimates for systems that behave ideally.

These correlations will be evaluated with respect to their accuracy and applicability. Since most of the compounds under investigation are nonpolar, the correlations should permit reasonable estimates. Methods that are less empirical and more broadly applicable are preferred over highly specialized developments.

It is worthwhile to review a few of the recent corresponding-states studies. While not directly applicable to this analysis, these studies show the trend in the extension of the corresponding-states approach. Extension of the empirical techniques used in the petroleum industry has proved inadequate for use in predicting coal fluid transport properties. Tsonopoulos et al.²² found a three-parameter corresponding-states model to be superior to an empirical (API-type) correlation for the prediction of high-temperature coal-fluid viscosities. The corresponding-states model was applied to pseudocomponents that were characterized by boiling-point cut. The critical properties and acentric factor were estimated,²³ and a simple mixture rule was applied. The corresponding-states model of Wilson et al. was similar, in principle, to that of Letsou and Stiel, but involved much more complicated functions of the correlating parameters. The average deviation of predicted values from experimental data was found to be 16%.

To obtain better predictive accuracy, Starling et al.²⁴ are developing higher-order (fourth- and fifth-parameter) corresponding-states models that attempt to deal with the polar and associative properties

exhibited by coal fluids. To date, their analysis has been restricted to the modeling of thermodynamic properties of pure compounds. Extending this technique to include transport properties and mixtures should not pose fundamental problems. Starling proposes the use of a reduced dipole moment (μ_r) to account for polar effects and a normalized latent heat (α) to account for associative properties.

The form of the correlations used by Starling is similar to that used in many corresponding-states studies:

Four-Parameter

$$Z = \text{compressibility factor} = Z_0(T_r, \rho_r) + \omega_s Z_\omega(T_r, \rho_r) + Z_\mu(T_r, \rho_r, \mu_r) \quad (19)$$

Five-Parameter

$$Z = \text{compressibility factor} = Z_0(T_r, \rho_r) + \omega_s Z_\omega(T_r, \rho_r) + Z_\mu(T_r, \rho_r, \mu_r) + \alpha \cdot Z_\alpha(T_r, \rho_r) , \quad (20)$$

where Z_0 , Z_ω , Z_μ , and Z_α are universal functions of the dependent variables listed in parentheses.

The four-parameter correlation seems to predict properties of polar compounds accurately. Vapor-pressure predictions for a set of 17 polar, aromatic compounds averaged approximately 2% deviation from the experimental values. Similar predictions for associating compounds using a five-parameter model were shown to exhibit an average deviation of 6% from experimental values.

Both the Tsonopoulos and the Starling studies emphasize the importance of applying corresponding-states principles to develop general correlations of broad utility. The higher-order models are relatively new. Subsequent development should result in more accurate correlating functions and more practical correlating parameters.

Light Scattering

This section outlines the major areas of physical significance to the experimental program. The discussion is restricted to the dilute solutions of uniform, monodisperse, spherical particles residing in a transparent medium. The references listed offer a more detailed treatment of the subject.

Light that is scattered in a perfectly homogeneous medium tends to interfere destructively such that no net scattered field is observed. Scattered light is a direct consequence of dielectric fluctuations (heterogeneities) in the scattering medium. With properly controlled experiments (that closely model idealized systems), we can relate the scattered-light signal to the physical properties that control the phenomenon causing the fluctuations. In the case of colloidal particles suspended in a pure fluid, this phenomenon is Brownian motion.

Brownian motion theory.^{6,25,26} The phenomenon of Brownian motion can be observed in particles that are relatively large (diameter, $\sim 1 \mu\text{m}$) on the molecular scale. The intensity of scattered light from a fluid is greatly enhanced by the addition of colloidal (seed) particles. This light-scattering enhancement provides a valuable analytical tool. Particle motion can be investigated by analyzing the light scattered from a seeded sample of fluid.

Consider the particle motion as being maintained by collisions with molecules of the medium and retarded by the effect of viscous drag. The scattered-light signal is modulated by the particle motions. The Brownian motion of a free particle (i.e., no applied force field) is described by the Langevin equation:²⁵

$$\frac{d\bar{u}}{dt} = -\beta\bar{u} + \bar{A}(t) , \quad (21)$$

where

\bar{u} = particle velocity vector,

t = time,

β = coefficient of dynamic friction, and

$\bar{A}(t)$ = fluctuating influence of molecular collision process
characteristic of molecular Brownian motion.

For a spherical particle, the coefficient of dynamic friction is given by Stokes Law:

$$\beta = 6\pi a\eta/m , \quad (22)$$

where

a = particle radius,

η = fluid viscosity, and

m = particle mass.

It is generally assumed that $\bar{A}(t)$ (1) is a random variable, (2) is independent of \bar{u} , and (3) varies on a much more rapid time scale than does $\bar{u}(t)$. The solution to the Langevin equation is a probability distribution since $\bar{A}(t)$ is a stochastic variable. The problem is essentially one of random walk statistics.²⁵ Therefore, the solution takes the form

$$W(\bar{u}, t; \bar{u}_0) ,$$

which specifies the probability of occurrence of velocity \bar{u} at time t , given that $\bar{u} = \bar{u}_0$ at $t = t_0$. The constraint that W approach Maxwellian distribution in T (temperature of fluid) as $t \rightarrow \infty$ allows us to proceed with the solution. Since Eq. (21) is linear and of first order,

$$\bar{u} - \bar{u}_0 e^{-\beta t} = e^{-\beta t} \int_0^t e^{-\beta t'} A(t') dt' . \quad (23)$$

By insisting that $W \rightarrow$ Maxwellian in T as $t \rightarrow \infty$, we find that²⁵

$$W(\bar{u}, t; \bar{u}_0) = \left[\frac{m}{2\pi kT(1 - e^{-2\beta t})} \right]^{3/2} \exp \left[\frac{-m \left| \bar{u} - \bar{u}_0 e^{-\beta t} \right|^2}{2kT(1 - e^{-2\beta t})} \right] . \quad (24)$$

Knowing the statistical velocity behavior of a Brownian particle, we can predict the nature of particle displacements since

$$\bar{r} - \bar{r}_0 = \int_0^t \bar{u}(t) dt , \quad (25)$$

where

$$\bar{r} - \bar{r}_0 = \text{displacement vector},$$

$$\bar{r} = \text{position vector at time } t, \text{ and}$$

$$\bar{r}_0 = \text{position vector at } t = t_0.$$

For times much greater than β^{-1} , we find that²⁵

$$W(\bar{r}, t; \bar{r}_0, \bar{u}_0) = (4\pi Dt)^{-3/2} \exp\left(-\frac{|\bar{r} - \bar{r}_0|^2}{4Dt}\right), \quad (26)$$

where

$$W = \text{probability of particle suffering a displacement to } \bar{r} \text{ at time } t, \text{ given that } \bar{u} = \bar{u}_0 \text{ and } \bar{r} = \bar{r}_0 \text{ at } t = t_0; \quad (26a)$$

$$D = \text{self-diffusion coefficient} = kT/(6\pi\eta a). \quad (26b)$$

The identification of D as the self-diffusion coefficient is an important relation developed by Einstein.²⁷ The equation for the self-diffusion coefficient [Eq. (26b)] is known as the Stokes-Einstein equation. The distribution function, W , will be useful in relating the particle motion to the light signal fluctuations.

Light-scattering theory.^{6,26,28} Our objectives in this area are to collect and to analyze the scattered light signal so as to relate the signal fluctuations to the motion of the suspended particles. The basis for characterizing these fluctuations is the autocorrelation function (see Fig. 1). The autocorrelation function of a signal is defined as the time average of the product of signals (otherwise identical) displaced by time τ :

$$\begin{aligned} A^*(\tau) &= \text{autocorrelation function} \equiv \langle A(0) A(\tau) \rangle \\ &\equiv \lim_{T \rightarrow \infty} \frac{1}{T} \int_0^T A(t) A(t + \tau) dt \equiv \lim_{N \rightarrow \infty} \frac{1}{N} \sum_{j=1}^N A_j A_{j+n}, \end{aligned} \quad (27)$$

and $\langle A \rangle = \text{time average of signal } A = \frac{1}{T} \int_0^T A(t) dt.$

A useful property of this function is its ability to characterize the period of fluctuation of a signal (Fig. 1). For values of τ , which are small compared with the signal period τ_s , $A(t) \sim A(t + \tau)$ and $A^* \sim \langle A^2 \rangle$. For times $\tau \gg \tau_s$, $A(t)$ and $A(t + \tau)$ are not correlated in any special way and $A^* \sim \langle A(0) A(\tau) \rangle \sim \langle A(0) \rangle \langle A(\tau) \rangle = \langle A \rangle^2$. Since $\langle A^2 \rangle$ is uniformly greater than $\langle A \rangle^2$, A^* will tend to decay from its maximum value of $\langle A^2 \rangle$ to its asymptotic ($T \rightarrow \infty$) value of $\langle A \rangle^2$ (Fig. 1).

The signal of interest in our system is the intensity (square of electric field = E_s^2) of the scattered light. By applying Maxwell's equations to our system, it is possible to show that the scattered electric field signal is proportional to⁶

$$E_s(t) \cong \sum_{j=1}^N \exp [i\bar{q} \cdot \bar{r}_j(t)] , \quad (28)$$

where

$\bar{r}_j(t)$ = position vector of j th particle at time t ,

\bar{q} = vector difference between incident and scattered propagation vectors,

$$|\bar{q}| = \frac{4\pi n}{\lambda_i} \sin \frac{\theta}{2} ,$$

n = medium refractive index,

θ = scattering angle, and

λ_i = incident wavelength.

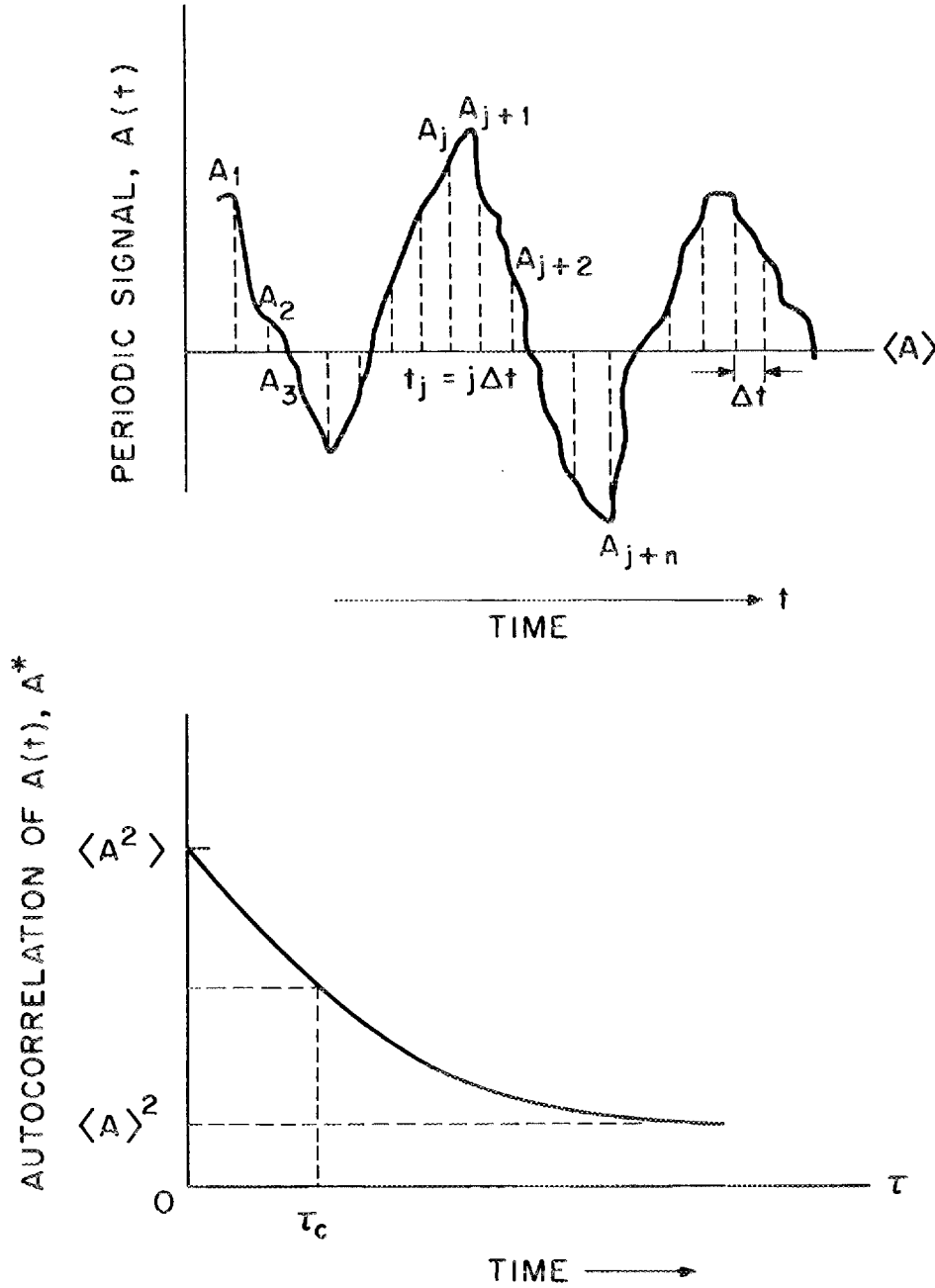


Fig. 1. Typical behavior of the autocorrelation function (A^*) of a periodic signal.

The autocorrelation function of the scattered electric field is proportional to:⁶

$$A_S^*(t) \equiv \sum_{j=1}^N \langle \exp(i\bar{q} \cdot [\bar{r}_j(t) - \bar{r}_j(0)]) \rangle, \quad (29)$$

where the sum $j = 1, \dots, N$ is conducted over particles present in the scattering volume at times t and $t = 0$.

It is evident that A_S^* is dependent on $[\bar{r}_j(t) - \bar{r}_j(0)]$, that is, the displacement of a particle in time t . This provides the link to Brownian motion theory. To determine the sum of individual particle contributions, we must calculate A_S^* based on properties averaged over the scattering medium and particle velocities.

Considering a generic particle, the normalized autocorrelation function of the scattered field is:

$$A_S^*/N = \iint \exp i \bar{q} \cdot \bar{r}_j(t) - \bar{r}_j(0) \cdot W(\bar{r}, t; \bar{r}_0, \bar{u}_0) \cdot P(\bar{u}_0) d\bar{r}_0 d\bar{u}_0, \quad (30)$$

where

W = function that predicts the occurrence of a particle suffering displacement $\bar{r} - \bar{r}_0$ within time t , given $\bar{r} = \bar{r}_0$ and $\bar{u} = \bar{u}_0$ at $t = 0$ [Eq. (26)];

P = function that predicts the probability of a particle having velocity \bar{u}_0 at $t = 0$;

= Maxwellian velocity distribution;

$$= \left(\frac{m}{2\pi kT} \right)^{3/2} \exp(-m |\bar{u}_0|^2 / 2kT); \text{ and} \quad (31)$$

N = number of particles in scattering volume \sim constant.

Performing the integration over r_0 and u_0 and making appropriate numerical approximations yields^{26,28}

$$A_S^* \cong \exp(-q^2Dt) = \exp(-t/\tau_c) , \quad (32)$$

where

$$q = \left| \vec{q} \right| = 4\pi n \sin(\theta/2)/\lambda_i ,$$

$$D = \text{diffusion coefficient} = kT/(6\pi a\eta) ,$$

$$\tau_c = \text{characteristic decay time} = (q^2D)^{-1} .$$

Note that A_S^* is a decaying exponential function of time (see Fig. 2).

Sometimes it is more practical to deal with the scattered-light signal in the frequency (ω) domain, rather than in the time domain. In this case,

$$A_S^*(\omega) = \frac{1}{2\pi} \int_{-\infty}^{\infty} A_S^*(t) e^{-i\omega t} dt \cong \frac{q^2D}{[\omega^2 + (q^2D)^2]} , \quad (33)$$

where $A_S^*(\omega)$ is a Lorentzian in ω (Fig. 2c) with half-width at half-maximum Γ ($\Gamma = q^2D$). This frequency distribution of the scattered light can be interpreted as the Doppler broadening of the incident (monochromatic) light due to the Brownian motion of the particles.

Equations (32) and (33) were developed along the classical lines, involving the autocorrelation function of the scattered field (E), (which was measured in early heterodyne experiments). In our case (homodyne experiment), we measure the scattered intensity (E^2). However, the results from heterodyne and homodyne experiments can be related if the electric field distribution is Gaussian (which is generally the case) and the central limit theorem is applied:⁶

TIME DOMAIN RESULTS

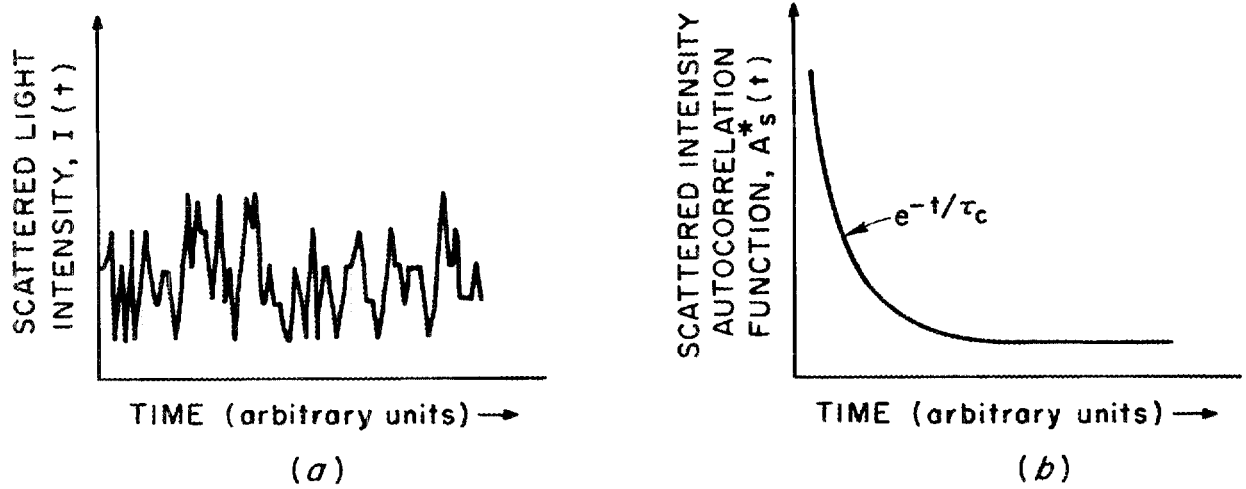
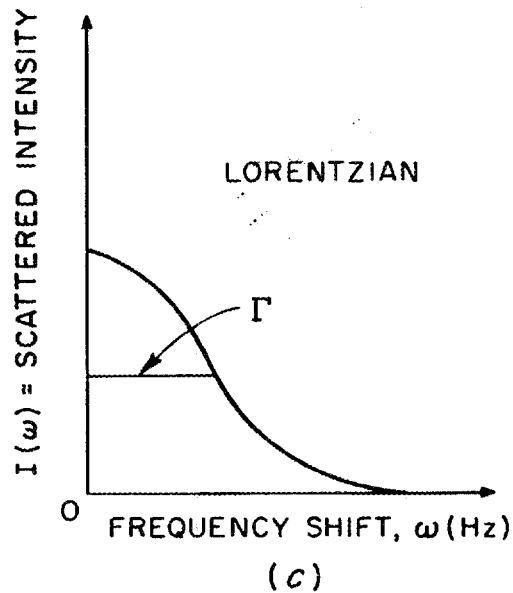
FREQUENCY DOMAIN RESULTS
(POWER SPECTRUM)

Fig. 2. Typical results from a dynamic light-scattering experiment.

$$\text{Homodyne} \approx \text{constant} + (\text{heterodyne})^2 \quad (34)$$

$$\langle E^2(o)E^2(t) \rangle = \left| \langle E(o)E(o) \rangle \right|^2 + \left| \langle E(o)E(t) \rangle \right|^2 \quad (34a)$$

$${}^2A_S^*(t) = \langle E^2(o)E^2(t) \rangle = C \cdot [1 + (\exp(-q^2Dt))^2] \quad (34b)$$

$${}^2A_S^*(t) \cong 1 + \exp(-2q^2Dt) \quad ; \quad \tau_c = (2q^2D)^{-1} \quad (34c)$$

$${}^2A_S^*(\omega) \cong [2q^2D / (\omega^2 + (2q^2D)^2)] \quad ; \quad \Gamma = 2q^2D \quad (34d)$$

Thus far, the discussion has been restricted to the ideal case of monodisperse spherical particles. Of course, no real systems are truly monodisperse. Even the widely used latex particles have a small, but appreciable, spread in size. It is important to consider the effect that polydispersity has on the data analysis. The signal from a polydisperse system contains a summation of exponentials, each with its own decay constant and associated scattering power:⁷

$$A_S^* = K \int_{r=0}^{r=\infty} [f(r) \cdot P(q,r) \cdot r^6 \cdot \exp(-t/\tau_1)] dr, \quad (35)$$

where

r = particle radius,

$f(r)$ = normalized distribution of particle size,

$P(q,r)$ = Mie scattering factor, $P \sim 1$ for $r \ll \lambda$, and

τ_1 = decay time for $r = r_1$.

The exact solution requires inversion of this equation to yield $f(r)$ directly. For complex signals, this is difficult to do accurately. Note that because of the r^6 dependence of the scattering power, large particles are more easily detected than small ones.

Many investigators analyze the signal via the cumulants method — a simpler manner that provides useful results. The cumulants method is the most widely used technique.²⁹⁻³¹ Consider that the signal coming from a polydisperse sample contains a distribution of line widths, where

$$\begin{aligned} G(\Gamma) &= \text{line width distribution} , \\ \Gamma &= \text{line width (Hz)} = (\text{decay time} = \tau_c)^{-1} , \end{aligned} \quad (36)$$

and

$$\int_0^{\infty} G(\Gamma) d\Gamma = 1 . \quad (37)$$

Koppel³¹ formulates his autocorrelation function as follows:

$$A_S^* = \int_0^{\infty} G(\Gamma) \exp(-\Gamma t) d\Gamma . \quad (38)$$

The analysis consists of estimating the behavior of $G(\Gamma)$ by expanding $\exp(-\Gamma t)$ about its mean value, $\bar{\Gamma}$. By definition:

$$\bar{\Gamma} = \int_0^{\infty} \Gamma \cdot G(\Gamma) \cdot d\Gamma , \quad (39)$$

and the moments (of order n) are defined as

$$\mu_n = \int_0^{\infty} G(\Gamma) \cdot (\Gamma - \bar{\Gamma})^n d\Gamma . \quad (40)$$

Expanding $\exp(-\Gamma t)$ in a Taylor series about $\bar{\Gamma}$, we obtain

$$\exp(-\Gamma t) = \exp(-\bar{\Gamma}t) \cdot \left[1 - (\Gamma - \bar{\Gamma})t + \frac{(\Gamma - \bar{\Gamma})^2 \cdot t^2}{2!} - \frac{(\Gamma - \bar{\Gamma})^3 \cdot t^3}{3!} + \dots \right]. \quad (41)$$

Substituting this expression into the equation for the auto-correlation function will result in

$$A_S^* = \exp(-\bar{\Gamma}t) \left(1 + \frac{\mu_2 t^2}{2!} - \frac{\mu_3 t^3}{3!} + \dots \right). \quad (42)$$

The terms involving μ_2, μ_3, \dots are assumed to be small corrections, allowing the approximation $\ln(1+x) \cong x$. Therefore,

$$\begin{aligned} \ln(A_S^*) &= -\bar{\Gamma}t + \frac{\mu_2 t^2}{2!} - \frac{\mu_3 t^3}{3!} + \dots \\ &= -\bar{\Gamma}t + \frac{1}{2!} \frac{\mu_2}{\bar{\Gamma}^2} (\bar{\Gamma}t)^2 - \frac{1}{3!} \frac{\mu_3}{\bar{\Gamma}^3} (\bar{\Gamma}t)^3 + \dots \end{aligned} \quad (43)$$

The form of $\ln(A_S^*)$ is a polynomial in t with the coefficients representing different properties of the line width distribution. The linear and quadratic terms, which are the most significant, are readily measured in most experiments. Higher-order terms are increasingly difficult to obtain experimentally and have less physical significance.

The linear term is the average line width as defined in Eq. (43). Since the scattering power of individual particles is skewed heavily toward large particles [Eq. (35)], this "average" $\bar{\Gamma}$ will result in "average" diameters weighted toward the largest species. This average

line width has a more straightforward interpretation when applied to measuring polymer diffusion coefficients.²⁹ The scattering is restricted to the Rayleigh regime (particle size \ll wavelength), and the scattered intensity is assumed to be proportional to the square of the molecular weight. This results in

$$\frac{\bar{\Gamma}}{q^2} = \frac{\sum N_i M_i D_i}{\sum N_i M_i} = \bar{D}_z, \quad (44)$$

where

\bar{D}_z = translational average diffusion coefficient,

N_i = concentration of polymers with $M = M_i$,

M_i = molecular weight,

D_i = diffusion coefficient of polymer with $M = M_i$.

The second moment (μ_2) normalized by the square of the average line width ($\mu_2/\bar{\Gamma}^2$) provides us with a polydispersity parameter. For a perfect monodisperse suspension, $\mu_2/\bar{\Gamma}^2 = 0$. In practice, values of $\mu_2/\bar{\Gamma}^2$ that are less than 0.1 are taken as an indication of a narrow distribution.

It is readily apparent that a quadratic regression analysis of $\ln[A_s^*(t)]$ vs t will provide estimates of $\bar{\Gamma}$ and $\mu_2/\bar{\Gamma}^2$. Using the Stokes-Einstein relation [Eq. (26b)], we obtain the viscosity directly, since

$$D = \bar{\Gamma}/2q^2 \quad (45)$$

and

$$\eta = kT/(3\Pi\mu Dd_p) . \quad (46)$$

Recent studies. The development of this analysis is similar to that used by most polymer and colloid scientists who are concerned with dynamic light scattering. The most common research area involving quasi-elastic scattering from particles uses fluids of known viscosity to determine the effective particle size of suspended solids. Only a few recent studies have used light scattering as a tool for investigating fluid viscosity, and all of them have been restricted to relatively low temperatures (near ambient).

The focus of these investigations has been to study the behavior of fluids during some particular phenomenon. Lyons et al.⁴ used light-scattering signals from 0.31- μm Teflon spheres to investigate the viscosity behavior of a critical binary mixture (47.8% nitroethane-isooctane) as it approaches the critical solution point from the one-phase region. Lyons' data were reported to a precision corresponding to an average relative error of $\pm 1\%$. His findings reinforced earlier studies which reported that a logarithmic divergence of the viscosity is observed as the critical point is approached.

Sorenson et al.⁵ utilized light scattered from Ludox (SiO_2 , 0.19- μm diam) particles to investigate the behavior of the fluid viscosity in the presence of a thermal gradient. The viscosity of water was found to be relatively unaffected by the applied thermal gradient. The results of their study tend to refute earlier work which suggested a large change in fluid viscosity due to the effects of a thermal gradient. Because of the added complication of the thermal gradient experiment, Sorenson reported his data as accurate to within $\pm 5\%$.

The most recent work involving viscosity measurement was performed by Saad and Gulari³² at Wayne State University. The n-heptane/CO₂(l) system was studied at saturation conditions over the temperature range from 10° to 50°C (1 to 8 MPa). The primary emphasis of this study was the measurement of the diffusivity of CO₂ in n-heptane. Viscosity was investigated because of its importance in relation to the diffusion analysis. Inverse micelles of bis(2-ethylhexyl)-sulfosuccinate (AOT) were used as seed particles. Samples contained 5 wt % AOT.

Measurements in pure heptane revealed that the diameters of the micelles shrink from 3.1 nm at 20°C to 2.9 nm at 60°C. An average diameter of 3.0 nm was assumed for all binary calculations. Experimental sources of error were not considered in any detail. Viscosity results were reported with a precision ranging from 0.5% at low temperatures and low CO₂ contents to as high as 20% at high CO₂ contents. Reported errors of about 10% were typical. No literature data are available for comparison. The reported values seem reasonable in light of the pure component viscosities, but the rather high surfactant concentration (5%) and the uncertain micelle stability may adversely affect the measurements. In their conclusion, Saad and Gulari state: "The reliability of the viscosity values obtained depends heavily upon the assumption that the micelles are of known uniform size and that there are no interactions between the scattering micelles."

This article points out the importance of using systems that conform to ideal models. The use of dilute, stable seeds is critical. Careful selection of the seed will help to eliminate ambiguity in the interpretation of results.

II. EXPERIMENTAL

Strategy-Seed Particles and Colloidal Stability

Systems that conform to relatively ideal models must be used to facilitate the interpretation of light-scattering results. Complications that result from elaborate data analysis should be avoided. The ideal system that was considered in this study has the following properties:

1. Seed particles are physically and chemically stable at the conditions of interest.
2. The particles are small (submicron) and relatively monodisperse.
3. The seed behaves as a "free particle" according to the Langevin equation; there are no significant influences from external forces (gravity, electrostatic, or particle-particle interaction).
4. The seed must exhibit colloidal stability (i.e., no particle aggregation).

The first requirement is fairly obvious. The hydrodynamic particle size must be known in order to infer viscosity from the Stokes-Einstein equation [Eq. (46)]. If the particle size varies in an unpredictable fashion, the measured viscosity has little validity. This requirement rules out most polymers as high-temperature seeds. Although some polymers do exhibit high-temperature stability, their conformation in a variety of solvents (at various temperatures) is rarely known. The scattering power of polymers in "good" solvents is also somewhat weak. In addition, one must consider the effect of the polymer on the solution viscosity. Therefore, attention is focused on inorganic particles that exhibit high-temperature stability in organic media.

The particles should also be relatively monodisperse to allow direct analytical techniques (cumulant analysis) to yield reproducible results. The signal must generally be described by a monodisperse model even if the seed is not strictly monodisperse. The synthesis of uniform latex spheres by emulsion polymerization represents the most advanced technique for producing model colloids. Even the latex spheres have a slight spread in size. Although few inorganic methods can rival the sophistication of emulsion polymerization, some methods have been developed for synthesis of suitable uniform aqueous sols of metal-oxide particles.^{33,34}

To satisfy the assumptions of the Langevin equation, we must work with dilute sols (parts-per-million level). Concentration effects can be detected by performing a series of experiments at different dilutions. In general, the effect of gravity is insignificant for particles smaller than $\sim 0.5 \mu\text{m}$ suspended in liquids. Stokes Law imposes a more precise limit on this size for specific conditions.²⁵

The last requirement is the least obvious and also the most difficult to satisfy. Colloid stability involves the action of repulsive forces to overcome the inherent attractive forces that exist between particles in suspension.^{35,36} Dipole interactions and London forces are always present and provide for the inherent instability of colloidal suspensions. In aqueous (polar) media, stabilization is achieved by electrostatic repulsion due to adsorbed ions. This mechanism is generally not as effective in nonpolar organic media.³⁵

Steric stabilization of "particles" in nonpolar media was developed in order to suspend various pigments and polymers in different solvents for use in the paint industry.^{35,37} The technique uses steric barriers

to prevent particles from coming into contact with each other. Typically, one end of a polymer is adsorbed onto the particle surface. The remaining polymer chain is not anchored and projects radially from the surface. The unanchored portion of the polymer is selected so that it will dissolve in the solvent and repel polymer chains of other particles. The theory describing the polymer-polymer interaction is well developed,^{35,36} and the principles governing the choice of stabilizers has been formulated.³⁵

The primary requirement of a stabilizer is for the unanchored portion to be very soluble in the suspending medium. This compatibility can be assessed by using the Scatchard-Hildebrand Theory of Regular Solutions or the more involved analysis of Flory-Huggins.³⁸ The size of the solvated portion is usually not critical. Solvated species with chain lengths as short as 18 carbon atoms have been successful in preventing flocculation. However, because of the restrictions imposed by the adsorption process, most stabilizers are much larger than this. A-B block copolymers, the most common stabilizer type, contain an A-anchor group, which is very insoluble and is adsorbed on the particle surface, and a B-anchor group, which is solvated. Molecular weights in excess of 1000 are often required to ensure adequate anchor group insolubility. The soluble component must be approximately the same size; otherwise, the copolymer will precipitate instead of forming stable micellular solutions in the solvents. Hence, the physical adsorption of block copolymers requires much larger molecules than are necessary for steric conditions.³⁵

The anchoring of the polymer to the particle surface is also very important. Each solvated polymer must be strongly attached to the

particle surface; otherwise, desorption will occur under either stress or dilution. Strong bonding is even more important for the elevated temperatures involved in this investigation. More rugged stabilizers can be synthesized by chemically bonding the polymer to the particle surface. This avoids many of the weaknesses of physical adsorption, while requiring that a specific chemistry be developed.

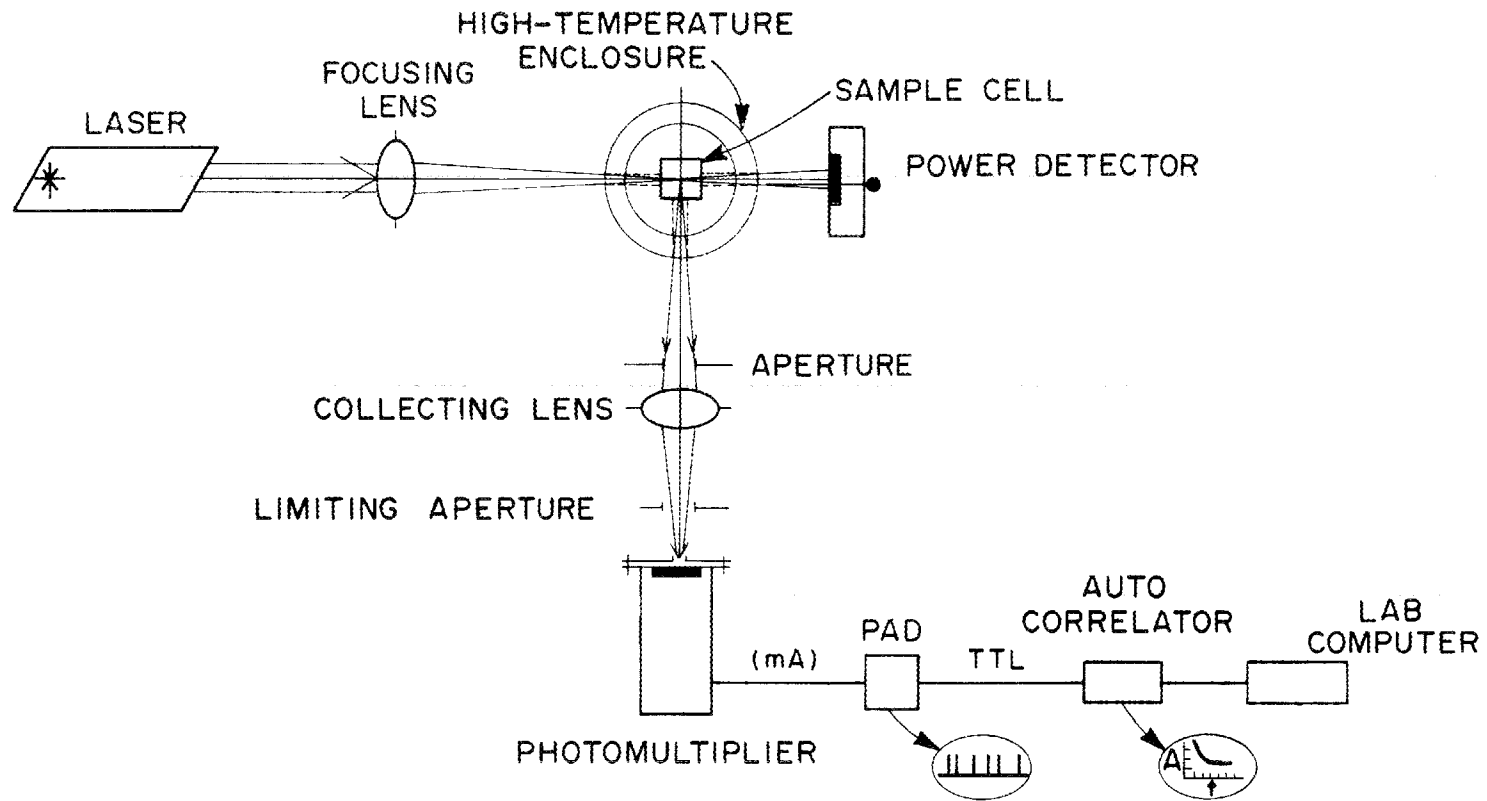
Finally, the particle surface should be fully covered with stabilizer in order to provide an enveloping barrier. It should be recognized that this polymer layer will affect the hydrodynamic radius determined by light scattering. However, if low-molecular-weight polymers are used, the size of the steric barrier can be kept to a very small fraction of the particle size. An 18-carbon-chain "polymer" (i.e., octadecane) represents only a 2% increase in the size of a 0.1- μm particle. Changes in the hydrodynamic diameter are even less significant, and conformation effects as a function of temperature will be of second order.

Apparatus

A custom-built dynamic light-scattering spectrometer is the centerpiece of this experiment. The apparatus (see Figs. 3 and 4) consists of a laser, source optics, sample enclosure, collection optics, detector, and signal processing equipment. Except for the high-temperature enclosure, the specification and assembly of components were based on established guidelines.^{7,28} The high-temperature enclosure was designed specifically for this study.

A 2-W argon-ion laser (Spectra Physics model 165-06) generates a vertically polarized beam ($\lambda = 488 \text{ nm}$) that is focused by a 150-mm plano-convex lens onto the center of the sample cell. The beam is focused to a

DYNAMIC LIGHT-SCATTERING SPECTROMETER



33



Fig. 3. Dynamic light-scattering spectrometer for high-temperature experiments.

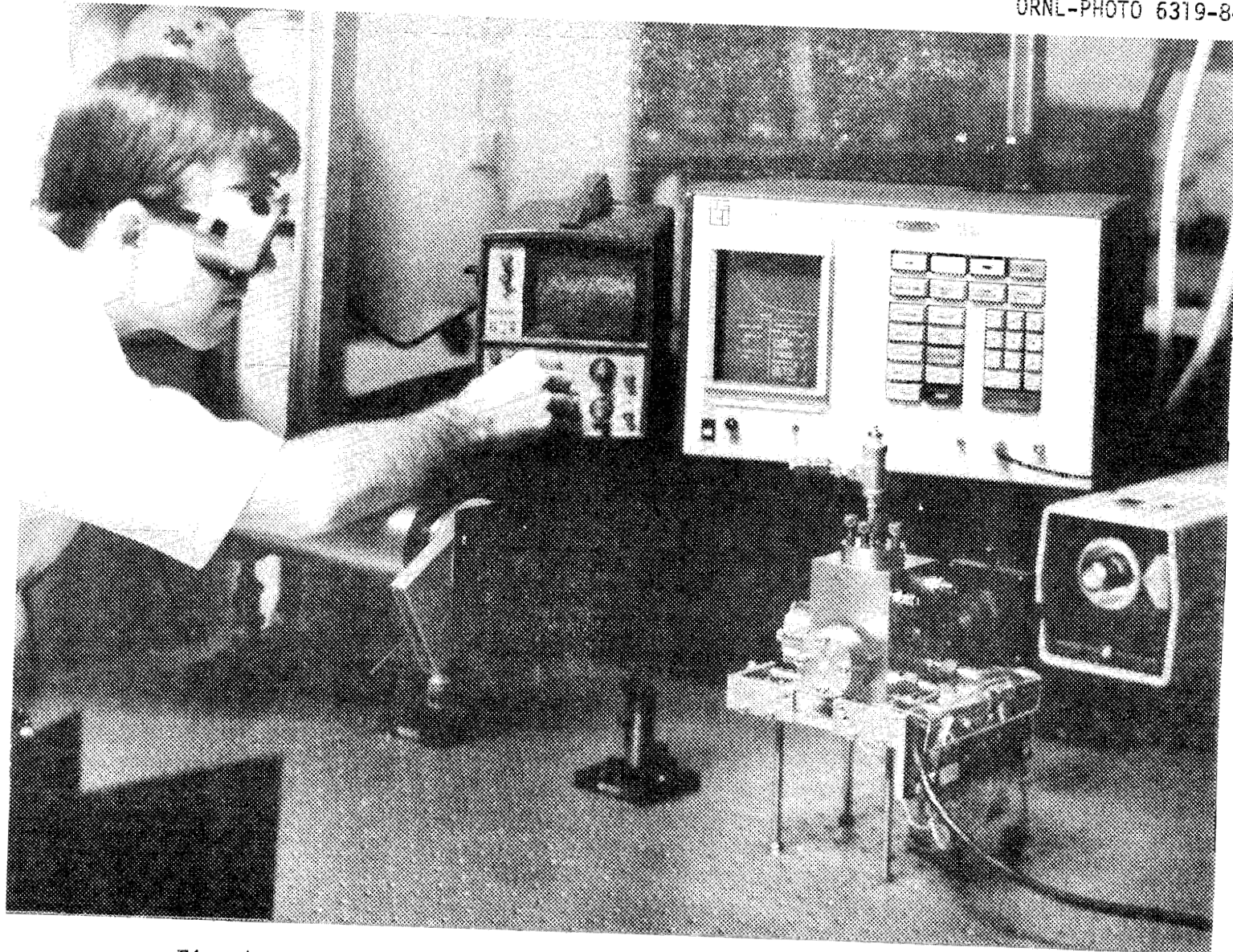


Fig. 4. Operation of the high-temperature spectrometer.

narrow width (~ 0.2 mm) to maximize the modulation of the scattered light (i.e., high signal/noise ratio). The axis of the lens is adjusted to be coincident with the source beam by using a micropositioner (Newport model LP-1). Typically only low-power operation (< 100 mW) is necessary.

The high-temperature enclosure (see Figs. 5-7) provides for temperature control of the sample to 500°C and pressurization to 1000 psi. The body of the enclosure is a $3 \times 3 \times 4$ in. stainless steel block. Quartz windows (Bond Optics, OPTISIL-3, 1.00 in. OD \times 0.75 in. thick, 40-20 finish) act as ports for the incident beam, the transmitted beam, and the light scattered at 90° . A top flange permits access to the sample cell, pressurization, and direct measurement of the fluid temperature (type K thermocouple). The entire block is insulated to minimize heat losses and thermal gradients. The window flanges and the top flange seal against O-rings. Reusable silicone rubber O-rings (Parker Nos. 2-012 and 2-020, 5604-70) are used for operation up to 300°C . Above 300°C , metal O-rings (Advanced Products No. EOI-00493-0307-1-SPD) are required. Standard fused-quartz spectrophotometer cuvettes are used as sample cells. Sample volumes of 3 mL are typical.

A control loop maintains the block temperature to within 0.1°C of the set point. A proportioning controller (Barber Coleman No. 5651-02033-0330) acts on a millivolt signal from a thermocouple located in the center of the block. The controller operates a power relay that supplies an adjustable voltage (0-120 Vac) to four 100-W cartridge heaters (Chromalux No. CIR-1060). A regulated argon gas cylinder provides the overpressure needed for high-temperature measurements.

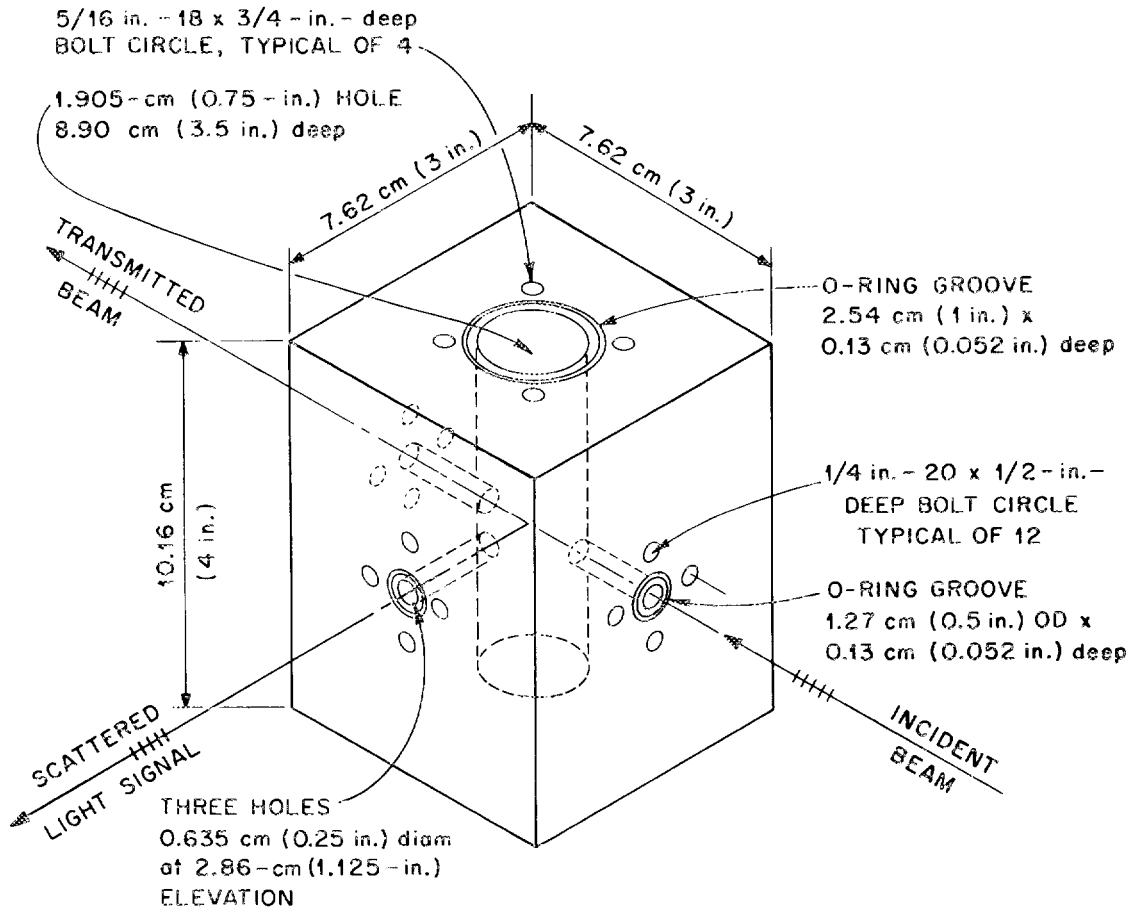


Fig. 5. High-temperature, high-pressure enclosure diagram (heater channels not shown).

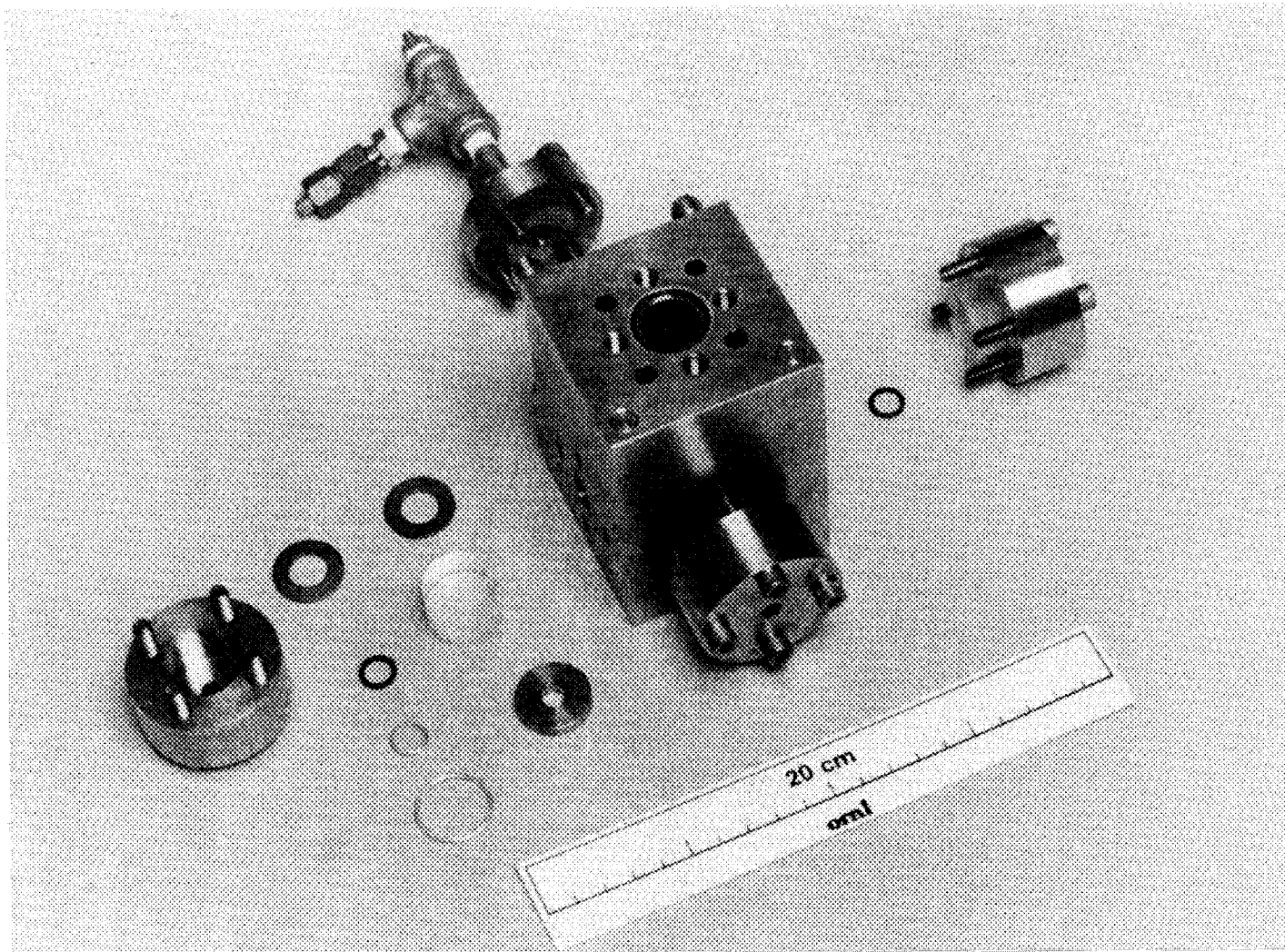


Fig. 6. Photograph of high-temperature, high-pressure enclosure — explosion view.

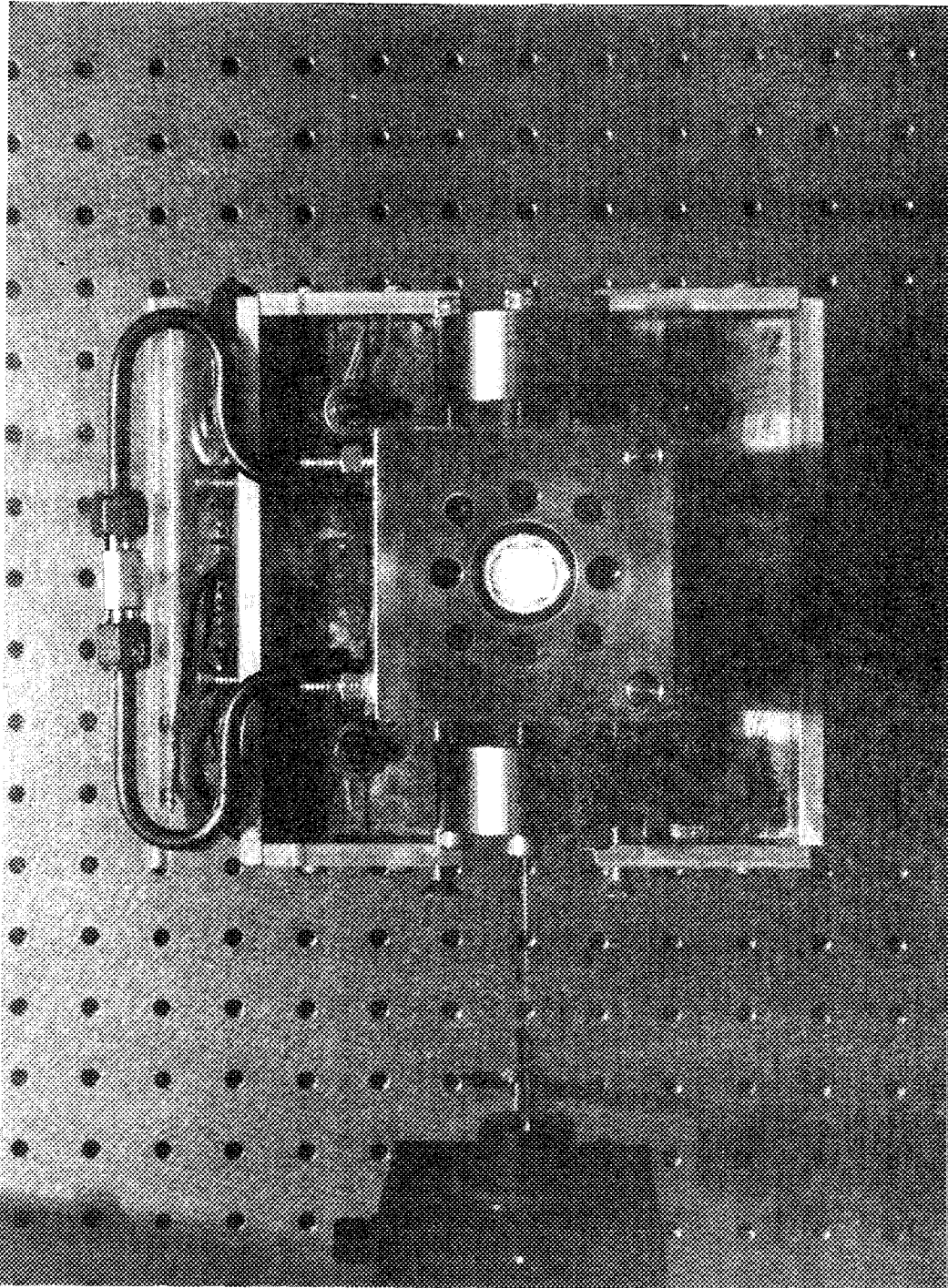


Fig. 7. High-temperature, high-pressure enclosure -- top view during operation.

The collection optics limit the light reaching the detector to that scattered at 90° from a small volume ($\sim 0.2 \times 0.2 \times 0.2$ mm). It is important that the scattering volume be kept small enough to ensure the coherence of the light that reaches the detector. Because of the destructive interference of components of different phases, incoherent light does not contribute to the signal. Guidelines for the sizing and placement of the limiting apertures have been reviewed in several articles.^{6,7,28} The first aperture is a small iris diaphragm (0.6 to 8 mm, Ealing No. 22-3305), located just in front of the imaging lens. A 100-mm plano-convex lens is placed ~ 8 in. from the center of the sample cell. The final aperture is a precision adjustable slit (Oriel No. 7250, 0- to 3.2-mm opening, ± 0.1 mm) that is mounted vertically, just in front of the detector and in the plane of the image formed by the lens. All of the components are positioned along the axis normal to both the incident beam and the plane of polarization.

The detector is an end-window photomultiplier (EMI No. 9863B350) mounted in a housing that provides radio frequency and magnetic shielding (Pacific model 3262 RF). A stable power supply (Pacific model 204-03) generates the 2000-Vdc potential required for the photomultiplier (PMT). A photon striking the cathode behind the PMT entrance window causes an electron to be emitted. This electrical signal is enhanced by a factor of 10^6 in the subsequent dynodemultiplier section. Figure 4 illustrates the nature of the fluctuating PMT signal (on the oscilloscope) and the resulting exponential autocorrelation function.

The pulse amplifier discriminator [PAD (Langley Ford model PD-01)] converts the milliamp pulses generated by the PMT to TTL pulses (0-5 Vdc) for use in a digital correlator. Pulses resulting from spurious effects in the PMT are also eliminated by the PAD.

The autocorrelator (Langley Ford model 1096) is a sophisticated digital signal processor that can accurately approximate the ideal autocorrelation function given by Eqs. (27) and (34b). Details of the electronic and mathematical operation are given in the literature.^{16,39} The time scale that can be probed ranges from decay times of 1 μ s to 10 s. An RS-232 communications interface between the autocorrelator and a micro-computer (Apple IIe) permits automated operation, off-line analysis, and convenient data logging. Data and calculated results are stored on magnetic disk. Significant computer programs are documented in Appendix D.

Materials and Procedures

Preparation of organophilic sols. After testing a number of different methods for the preparation of organophilic sols, we found that the synthesis suggested by Van Helden et al.⁴⁰ was the most successful. Not only do the particles meet all the requirements mentioned previously, but the procedure is also relatively simple.

The preparation suggested by Van Helden et al. is actually a combination of an alcosol preparation developed by Stober et al.⁴¹ and a surface treatment developed by Iler.⁴² A monodisperse silica sol is formed by the controlled hydrolysis of ethyl orthosilicate (EOS) $[\text{Si}(\text{OC}_2\text{H}_5)_4]$ in an alcohol-ammonia-water mixture. The silica particles are rendered organophilic by chemically bonding stearyl alcohol

[$\text{CH}_3(\text{CH}_2)_{17}\text{OH}$] to the particle surface. The resulting particles form stable colloidal suspensions in a number of nonpolar aliphatic, cyclic, and aromatic solvents.

EOS is hydrolyzed in the presence of water, with ammonia acting as a catalyst. In a typical preparation, 5.4 mL of concentrated NH_4OH (28% NH_3) and 85 mL of absolute ethanol are mixed in a clean flask. EOS is added (3.54 g), and the reaction mixture is stirred at constant temperature (25°C) for at least 4 h. Within 15 min, a bluish-white opalescence can be observed, indicating the presence of uniform, sub-micron particles. Our standard recipe generally results in spherical particles with a diameter of 0.1 μm . The size of the particles can be controlled by varying the reactant concentrations. A small aliquot of the alcisol is normally reserved for analysis by light scattering. The alcisol particles are stabilized by electrostatic forces and remain in suspension for months.

Five grams of stearyl alcohol is added to the alcisol as a slurry, dissolved in 100 mL of ethanol. Absolute ethanol is then added to facilitate water removal by shifting the water content below the azeotropic composition. After the ethanol and the water are distilled at atmospheric pressure, a nitrogen blanket is introduced. The silica-stearyl alcohol mixture is heated to 190°C and maintained at that temperature for at least 3 h to complete the esterification reaction between the silica and the stearyl alcohol. Stearyl alcohol forms a Si-O-C linkage to the particle surface.

The modified silica is separated from the excess stearyl alcohol by sequential centrifugation. For the first separation, a 60/40 (v/v) mixture of chloroform and cyclohexane is added to the melt. Chloroform is

an excellent solvent for the excess stearyl alcohol, while cyclohexane lowers the density to a point where centrifugation of SiO_2 is practical. The supernate is discarded, and the process is repeated with the solvent of interest. Before centrifugation, sonication of the suspension is sometimes necessary to redisperse the particles and ensure good contacting. Normally, only three cycles are necessary to produce dispersions that are free of contaminants. High-quality reagents (99+%) are used without further purification.

Light-scattering measurements. The organophilic preparation results in a fairly concentrated suspension. Stock suspension is diluted with pure reagent in order to reduce the particle concentration. Particle interaction effects are minimized by diluting to a solids concentrations of <50 ppm. A preliminary light-scattering test with a low-temperature, low-power spectrometer (Langley Ford model LSA-6) is used to determine the particle concentration required to provide sufficient signal strength. The optics of this unit are fixed at a scattering angle of 90° . Preliminary tests also help to screen out samples that do not justify further study.

We follow the recommendations of Degiorgio and Lastokova⁴³ for the operation of the digital correlator. The sample time is selected so as to span about four decay times ($4 \cdot \tau_c$). Laser power and aperture settings are adjusted to provide good signal/noise ratios (coherent scattering) and strong signals. Several short (60-s), independent runs are superior to one long run. The average of the runs provides a more accurate estimate of the viscosity. The standard deviation of the runs also provides information about the reproducibility of the measurement. With optimized

operation and a stable sample, five replicate runs (60 s each) yield a coefficient of variation of the predicted viscosity of <1%.

Once the sample cuvette is aligned in the high-temperature enclosure, a base-line diameter is obtained at ambient conditions. This diameter, which is calculated on the basis of a predetermined low-temperature viscosity, is used in subsequent viscosity calculations. Measurements at higher temperatures are conducted only after the sample has thermally equilibrated with the enclosure (~15 min at temperature). High-temperature refractive indices are calculated using the standard Eykman equation (Appendix C).⁴⁴ The accuracy of this estimation method is >99%. An overpressure of at least 50% of the saturation pressure is applied for measurements conducted above the normal boiling point. Finally, after cooling, additional measurements at ambient conditions are made to check the stability of the sol. The initial and final results should correspond within 2%.

III. DISCUSSION OF RESULTS

Pure Components

The experimental results consist of an investigation of five non-polar compounds and two binary mixtures. The viscosities of n-pentane, n-heptane, cyclohexane, chloroform, and toluene were measured from room temperature up to ~90% of the critical temperature. An ideal mixture (pentane-heptane) and an interacting mixture (hexane-isopropanol) were also studied at elevated temperatures. Tests were subsequently performed to ensure the internal consistency of the results. Comparison of the experimental data with values found in the literature allowed an independent evaluation of the results to be made.

Since the stability of the microparticle diameter is a central issue, tests were conducted to confirm this assumption. Light-scattering runs were always repeated at least five times for each experimental temperature. Polydispersity coefficients (μ_2/Γ^2) were normally much less than 0.1, ensuring the validity of the cumulants expansion [Eq. (43)]. Averaged results for one temperature yield a mean value for viscosity and a coefficient of variation (CV) for the set of measurements. The repeatability of the measurements was generally >99% (CV).

The standard diameter (at 20°C) was also checked after operation at elevated temperatures in order to confirm the particle stability. The measurements generally agreed to within 2% (Table 1). A careful comparison of results for n-pentane also showed a close correspondence during the heating and cooling cycles (Table 2).

Table 1. Standard particle diameters (at 20°C) by light scattering before and after high-temperature operation

Solvent	Sample No.	Initial diameter (μm)	Final diameter (μm)	Variation ^a (%)
n-Pentane	3.115	0.1062	0.1064	0.19
	3.146	0.1084	0.1081	0.28
n-Heptane	3.149	0.134	0.1363	1.7
Cyclohexane	3.097	0.1093	0.103	6.1
	3.154	0.1026	0.1017	0.88
Toluene	3.087	0.1245	0.121	2.8
	3.153	0.1147	0.1133	1.2
Chloroform	3.112	0.114	0.1093	4.1
Pentane-heptane	3.152	0.1014	0.1021	0.69
Hexane-isopropanol	3.165	0.0645	0.0649	0.62

$$^a\% \text{ variation} = \frac{\text{initial} - \text{final}}{\text{initial}} \times 100.$$

Table 2. Typical viscosity measurements during corresponding heating and cooling cycles

(Sample No. 3.146, solvent = n-pentane)

Heating cycle		Cooling cycle	
Temperature (°C)	Viscosity (mPa·s)	Temperature (°C)	Viscosity (mPa·s)
20.0	0.2337	20.0	0.2334
61.1	0.1691	60.2	0.1692
80.5	0.1440	81.2	0.1452
90.4	0.1346	90.7	0.1348

Results from independent samples also show good agreement (Figs. 8 through 12). All of this information indicates that the nature of the microparticle suspension does not change significantly during the experiment. However, at temperatures above $\sim 0.9T_C$, the sols become unstable, agglomerated, and settled.

The basic experimental results are summarized in Table 3 and in Figs. 8 through 12. The experimental data are plotted in contrast to a standard Andrade correlation and the Letsou-Stiel corresponding-states prediction. The Andrade equation,¹⁸

$$\eta = A \exp [B/T] \quad (A \text{ and } B \text{ constants}), \quad (47)$$

is the standard form for correlating pure-component viscosity at temperatures below the normal boiling point. The constants A and B were obtained by regression of low-temperature data referenced in the figures. High-temperature data from other sources (when available) are also shown.

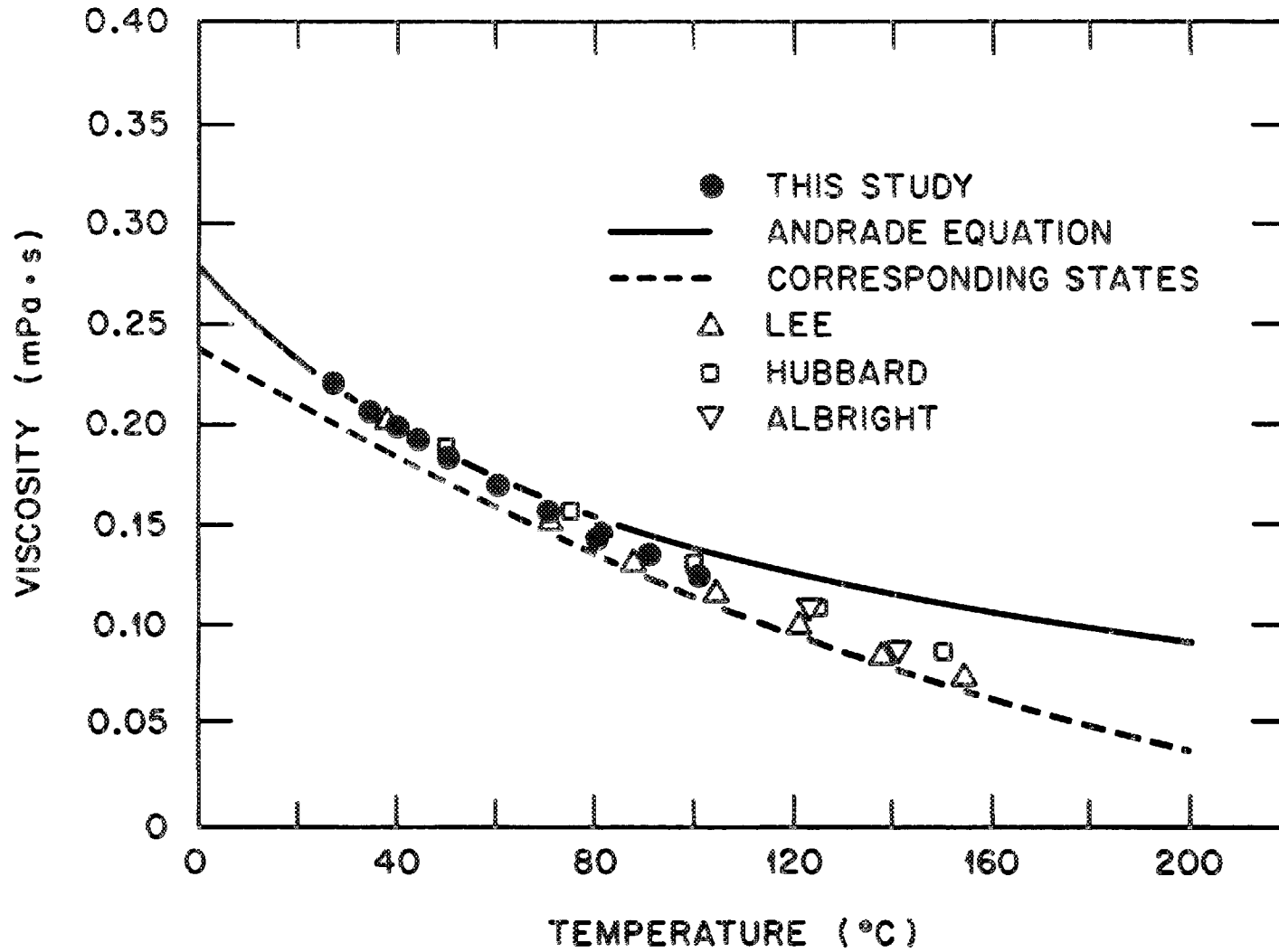


Fig. 8. Viscosity of n-pentane: experimental results, literature values, and predictions.

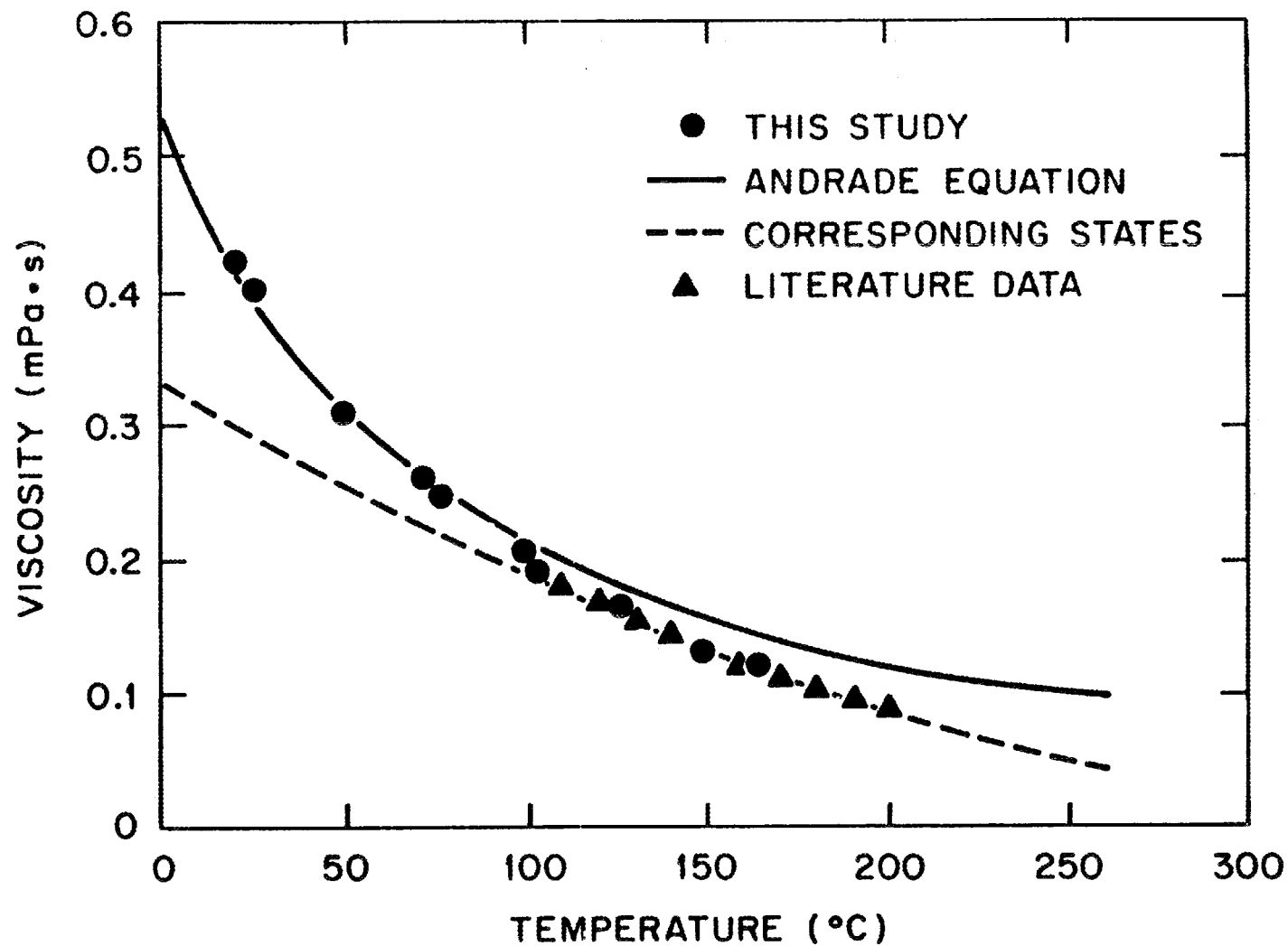


Fig. 9. Viscosity of n-heptane: experimental results, literature values, and predictions.

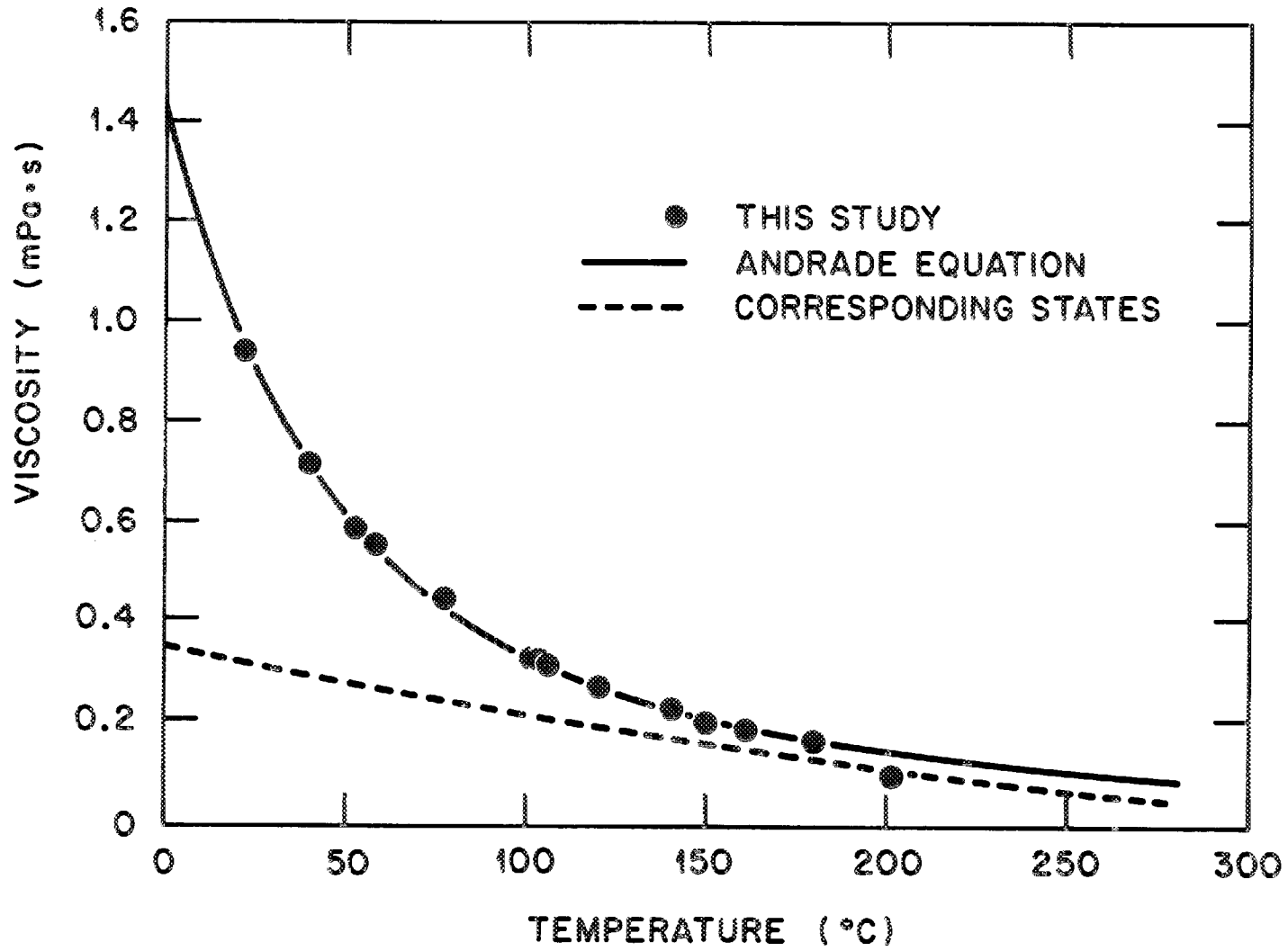


Fig. 10. Viscosity of cyclohexane: experimental results and predictions.

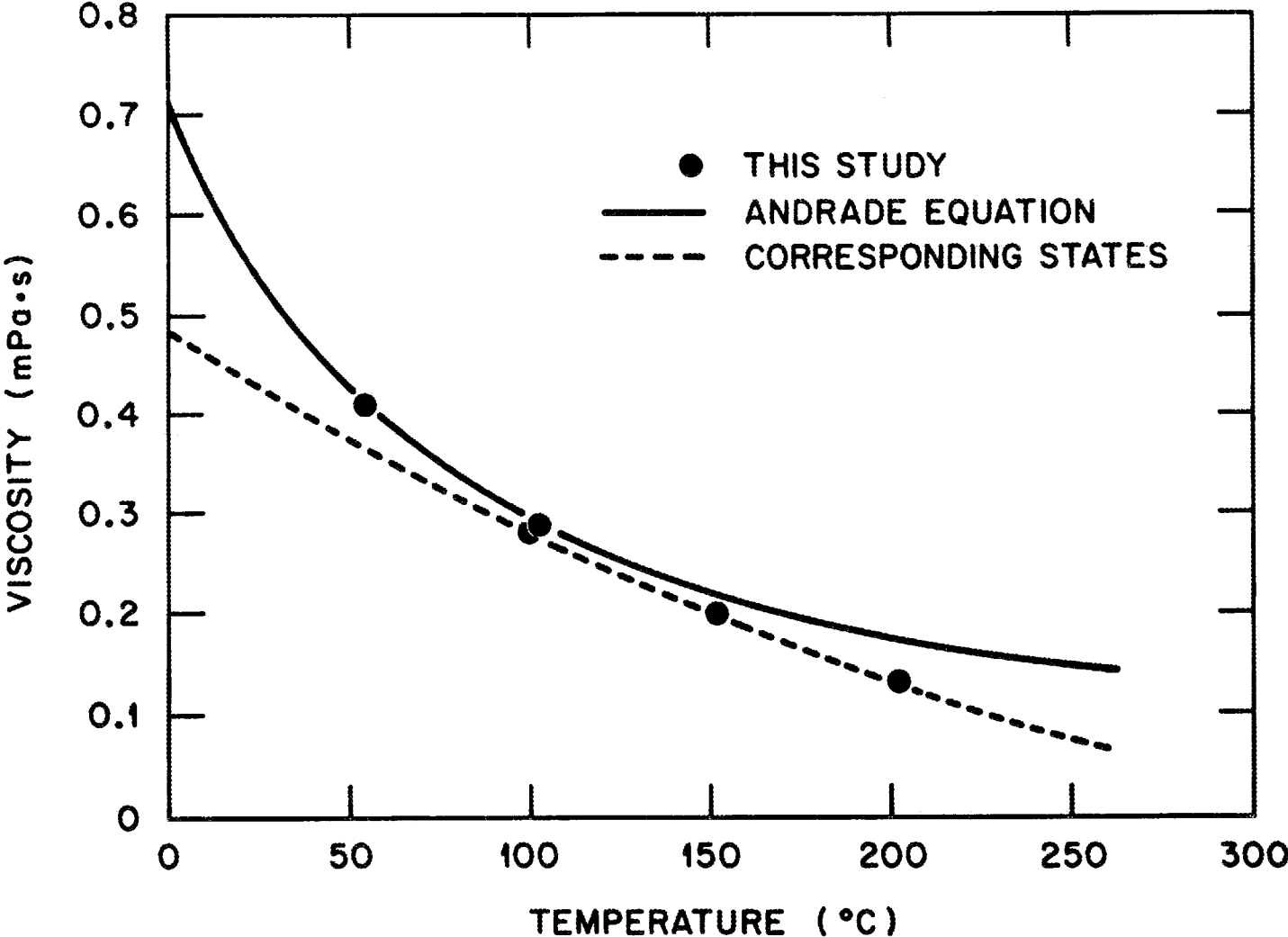


Fig. 11. Viscosity of chloroform: experimental results and predictions.

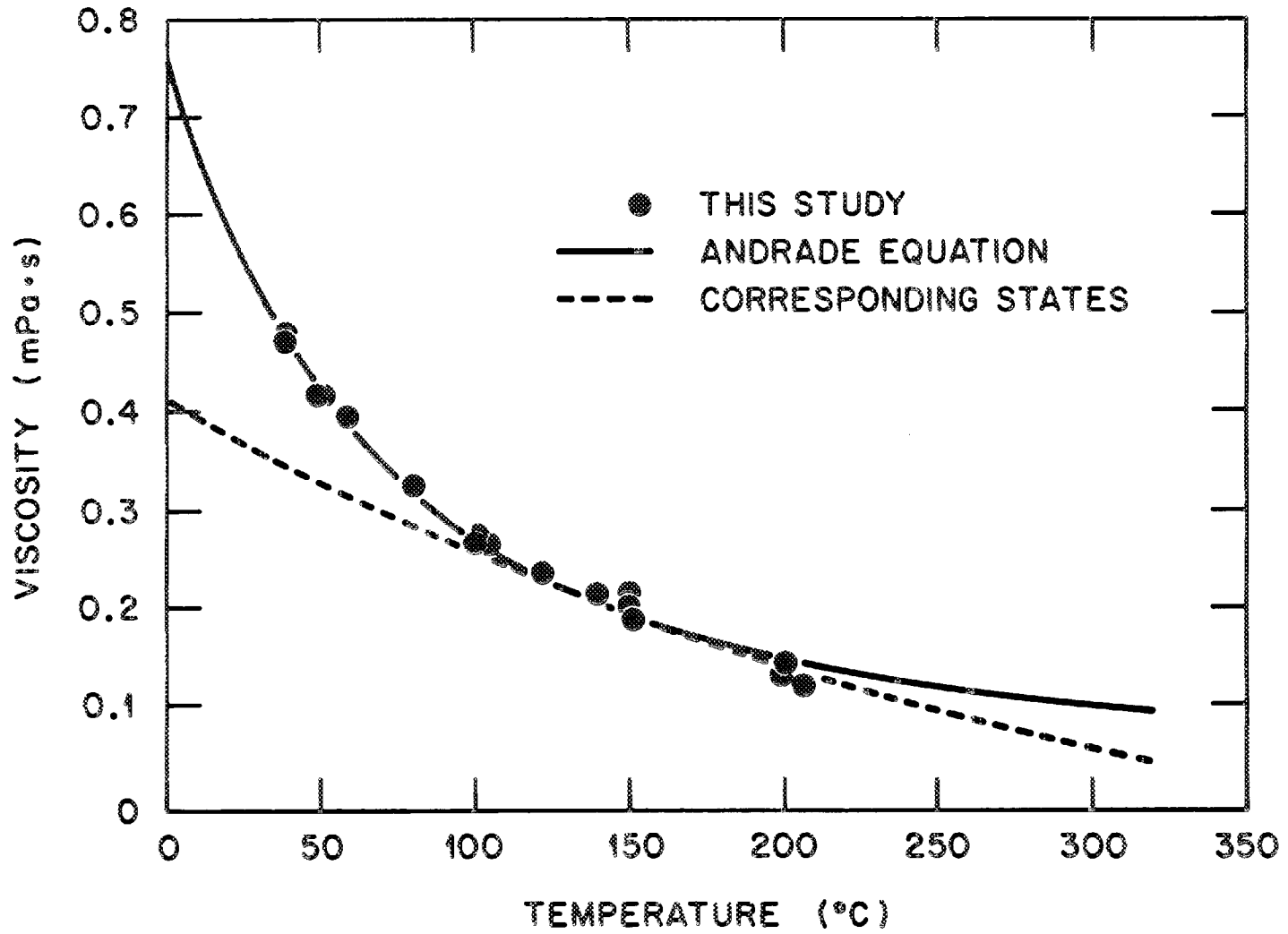


Fig. 12. Viscosity of toluene: experimental results and predictions.

Table 3. Comparison of viscosity data and recommended correlations

Compound	Average deviation from experimental values	
	Andrade equation, $T_r < 0.7$ (%)	Corresponding-states equation [Eq. (6)], $T_r > 0.7$ (%)
<u>n</u> -Pentane	0.67	7.1
<u>n</u> -Heptane	1.44	2.5
Cyclohexane	1.72	23.4
Chloroform	2.34	3.2
Toluene	1.77	4.8
Cumulative average	1.59	8.2
		(4.4%, excluding cyclohexane)

A number of general observations can be made after reviewing these figures. The low-temperature measurements are accurately characterized by the Andrade equation. At temperatures somewhat above the normal boiling point, the Letsou-Stiel predictions provide a more accurate representation of the data. This is exactly the type of behavior that one would expect. As the temperature increases, the assumptions inherent in the corresponding-states model are followed more closely. Polar (dipole) effects become less important, and any complex structural effects are diminished due to the randomizing influence of increased temperature. In general, the light-scattering results are in good agreement with literature data.

The results for n-pentane and n-heptane (Figs. 8 and 9) can be compared with the high-temperature values reported in the literature. The pentane data are well within the spread of values documented by Lee and Ellington.⁴⁵ The data for heptane correspond quite closely ($\pm 2\%$) to the high-temperature values found in the literature.⁴⁸

Results for cyclohexane, chloroform, and toluene (Figs. 10 through 12) are not readily compared with literature values at high temperatures. However, correspondence to the standard low-temperature values (Andrade equation) is excellent, and the high-temperature behavior is in agreement with the corresponding-states predictions. This agreement is especially close in the case of the chloroform results (Fig. 10). The results for toluene (Fig. 11) are similar in nature but somewhat more scattered. The transition from exponential behavior to corresponding-states behavior is less clear for the cyclohexane results (Fig. 12).

The predictions of the Lee and Ellington correlation require some extra consideration and explanation. The calculations of the Letsou-Stiel correlation are quite straightforward, requiring only the most common parameters (T_c , P_c , ω). In contrast, Lee's method depends on an uncommon parameter, ϵ , the volume expansion ratio at the triple point. Calculations are complex and are extremely sensitive to small changes in ϵ . Lee provides fitted values of ϵ (determined by regression of viscosity data) for a limited set of compounds. Fitted values of ϵ are given for n-pentane, n-heptane, and cyclohexane. Values of ϵ for chloroform and toluene were estimated by the method suggested by Lee (Appendix B). Table 4 demonstrates that the estimation methods do not provide a precise means of calculating optimum (i.e., "fitted") ϵ values.

Table 4. Lee's triple-point parameter, ϵ :
fitted, estimated, and calculated literature values

Compound	(1) Literature values	(2) Fitted values	(1) and (2) $\Delta\%$	(3) Estimated values	(2) and (3) $\Delta\%$
Benzene	1.134	1.101	3.0	1.112	1.0
Cyclohexane	1.051	1.07635	2.4	1.0982	2.0
<u>n</u> -Pentane	—	1.0402	—	1.0552	1.4
<u>n</u> -Heptane	—	1.0413	—	1.0145	2.5
Carbon dioxide	1.285	1.206	6.1	1.3085	8.5
Toluene	1.009	—	—	1.013	—
Chloroform	—	—	—	0.937	—

For example, the viscosity estimates for chloroform were much too large. The other Lee predictions are shown in Figs. 13 through 16. Estimates resulting from the use of fitted ϵ values provide accurate viscosities over a wide range of temperatures. Predictions using calculated or estimated values of ϵ are very unreliable. The results for toluene (Fig. 16) illustrate the inaccuracy of this method when fitted values of ϵ are not available.

The predictive validity of this correlation is questionable. An argument could be made that, while ϵ is a proper correlating parameter, its accurate estimation is difficult. Close examination of Lee's work reveals that fitted values of ϵ and the best experimental determinations of ϵ differ by as much as 6% (Table 4). This difference is significant in view of the sensitivity of the calculations to small changes in ϵ .

Lee's development is essentially empirical. The development of a single correlation for the viscosity of a fluid throughout the entire

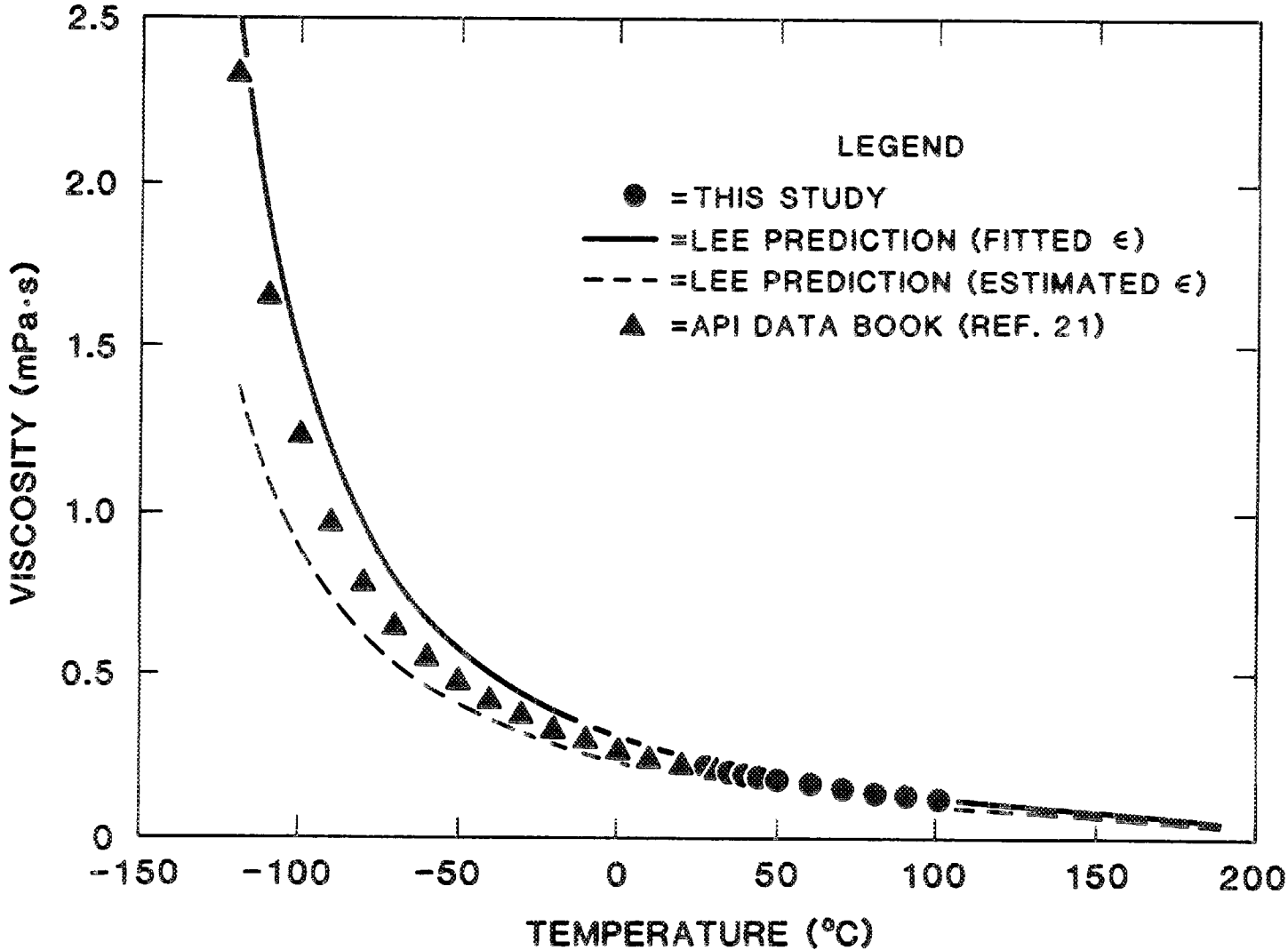


Fig. 13. Comparison of viscosity data and Lee predictions for n-pentane.

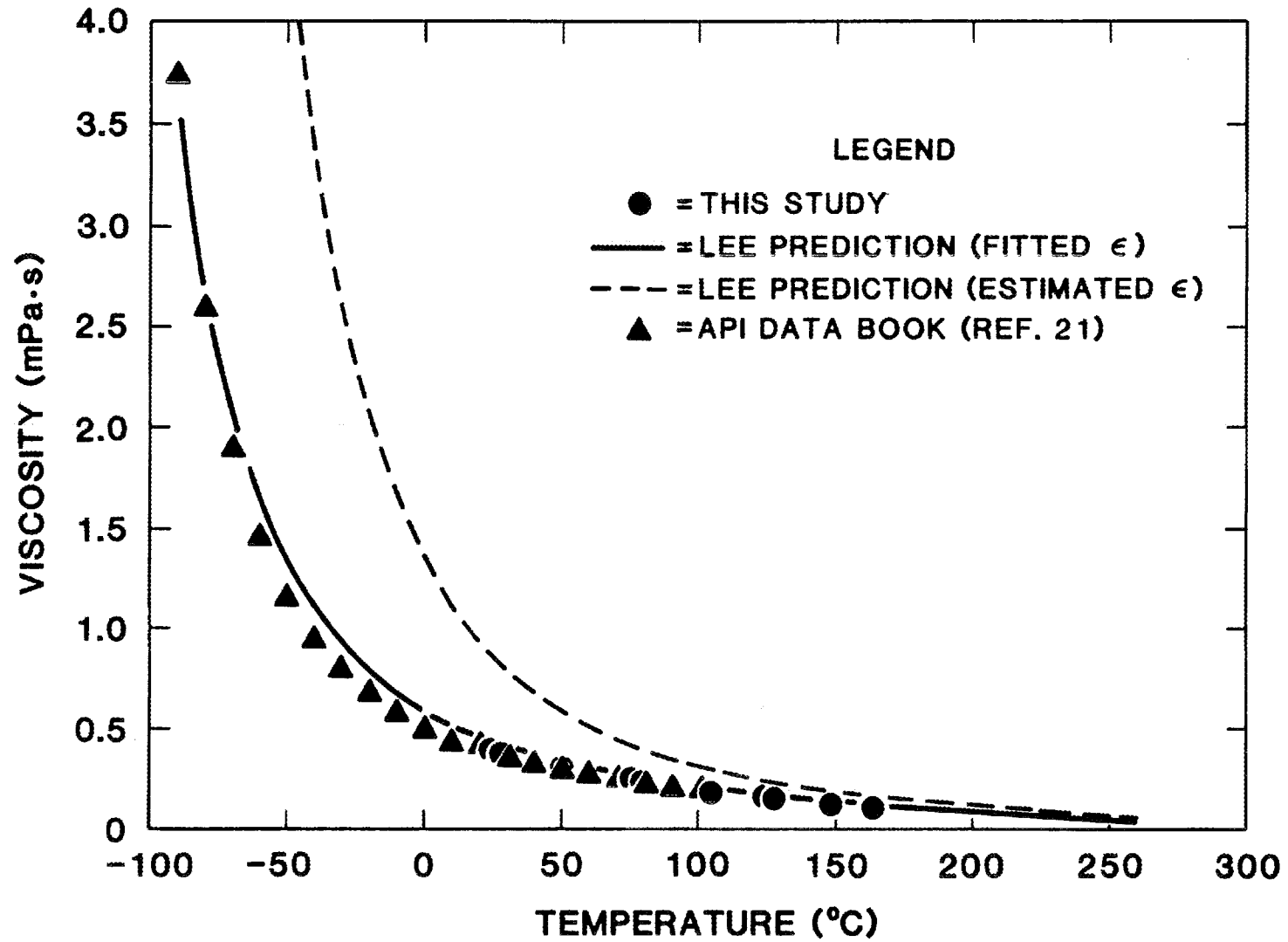


Fig. 14. Comparison of viscosity data and Lee predictions for n-heptane.

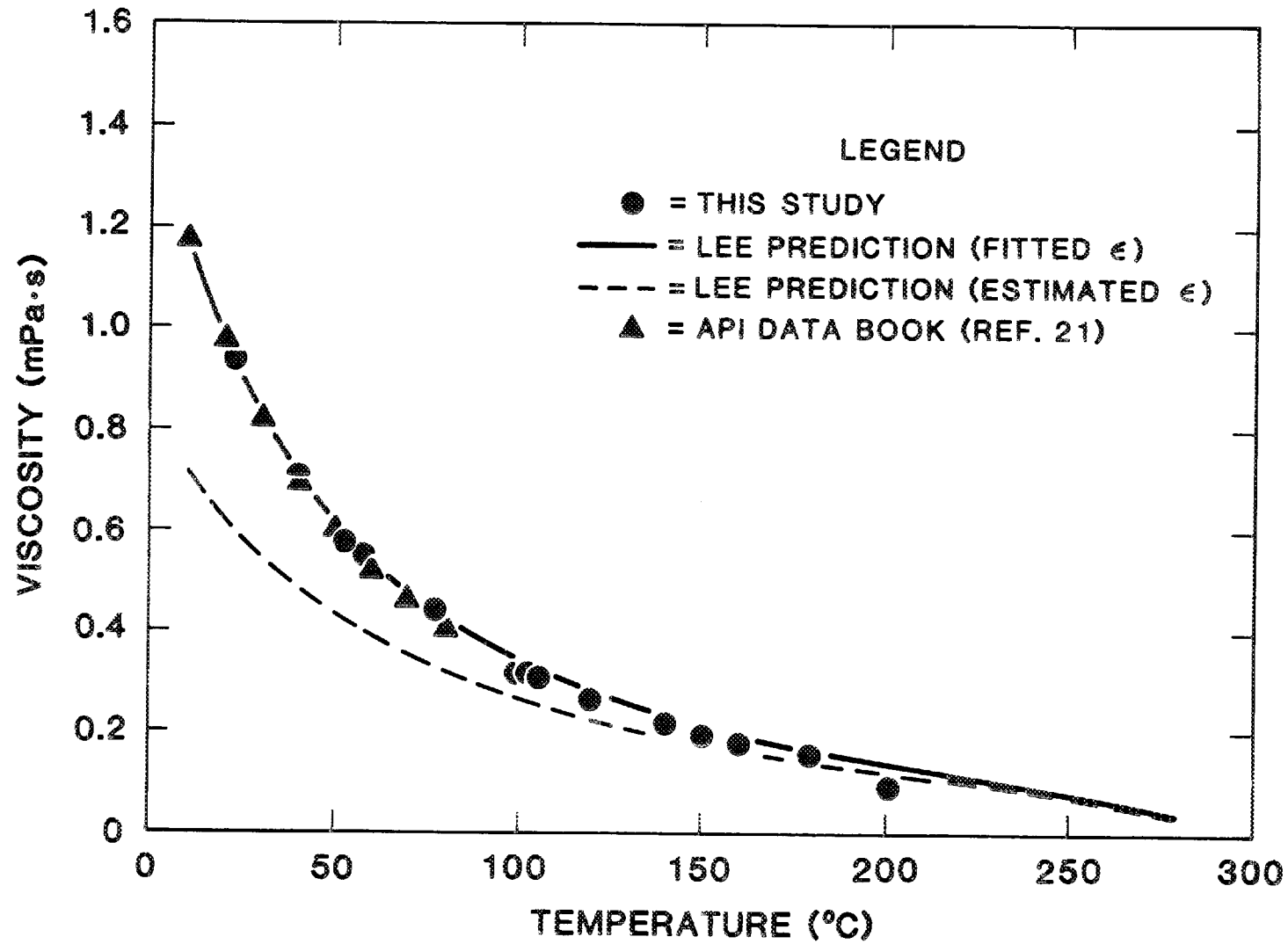


Fig. 15. Comparison of viscosity data and Lee predictions for cyclohexane.

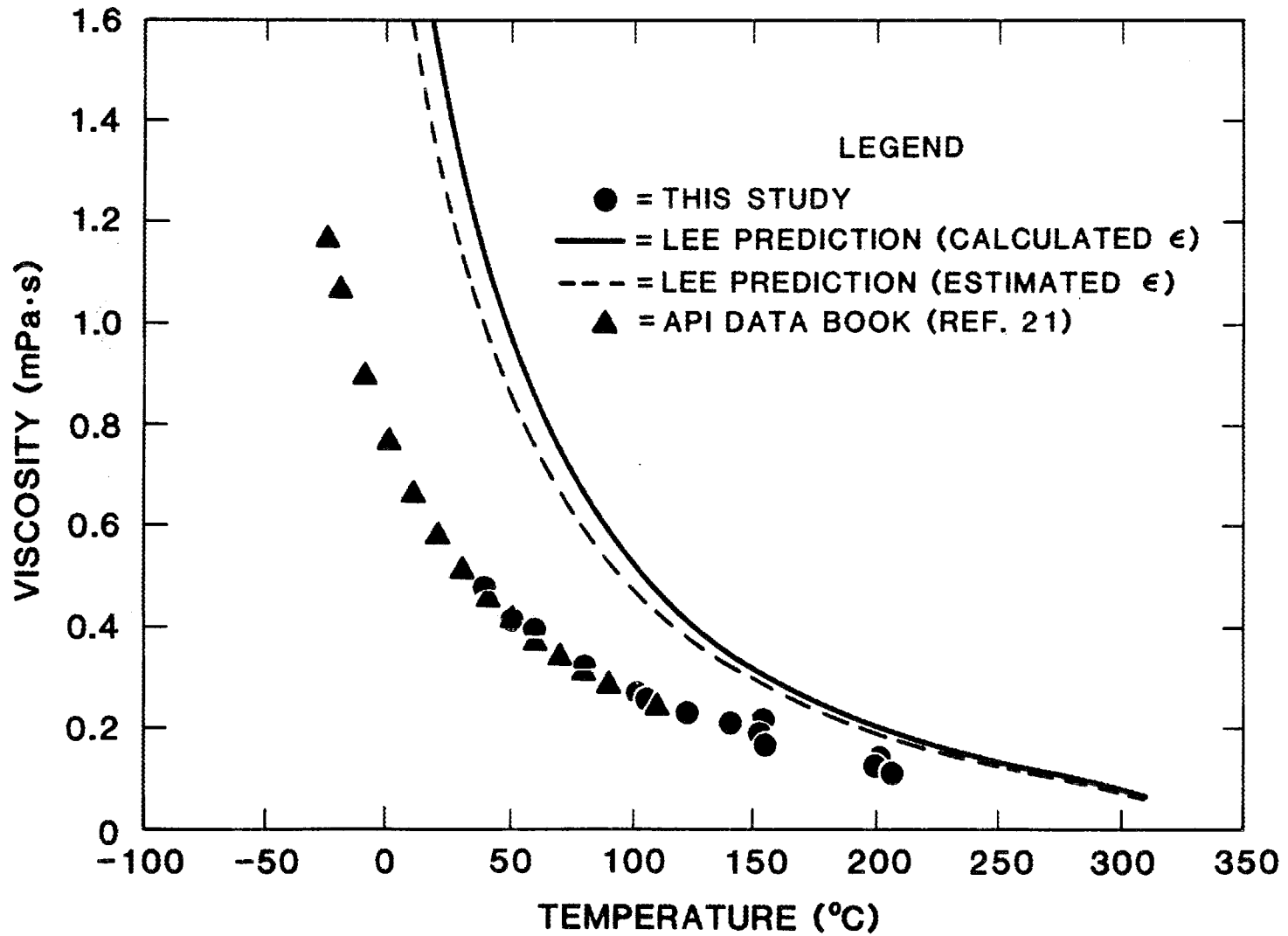


Fig. 16. Comparison of viscosity data and Lee predictions for toluene.

liquid range is significant; however, the predictive validity of this correlation is limited due to its empirical basis. A valid correlation over the entire liquid range must account for the vast differences in the nature of liquids near the triple point and the critical point. It is important that correlating parameters represent effects which have direct theoretical significance. The inordinate success of the original theory of corresponding states is evidence of this fact. Identification of truly significant liquid-state parameters is difficult since our theoretical knowledge is not advanced in this area. The three-parameter correlation of Letsou and Stiel remains the most broadly applicable predictive method for use at elevated temperatures.

Mixtures

A brief study of two model binary systems, an ideal mixture (50 mol % n-pentane/50mol % n-heptane) and an interacting mixture (75 mol % n-hexane/25 mol % isopropanol), was undertaken. The pentane-heptane system should conform to ideal behavior since both components are members of a homologous series and do not differ greatly in molecular size. Vapor-liquid equilibrium data indicate that the hexane-isopropanol system should exhibit large positive deviations from ideality. A minimum boiling azeotrope occurs at 61.5°C and a hexane mol fraction of 0.73.

The results for the ideal system are contrasted with two mixture correlations in Fig. 17. Pure-component viscosities were derived from this investigation. The Kendall equation represents the data very accurately over the entire temperature range. As in the case of the pure compounds, the corresponding-states model is accurate only in the

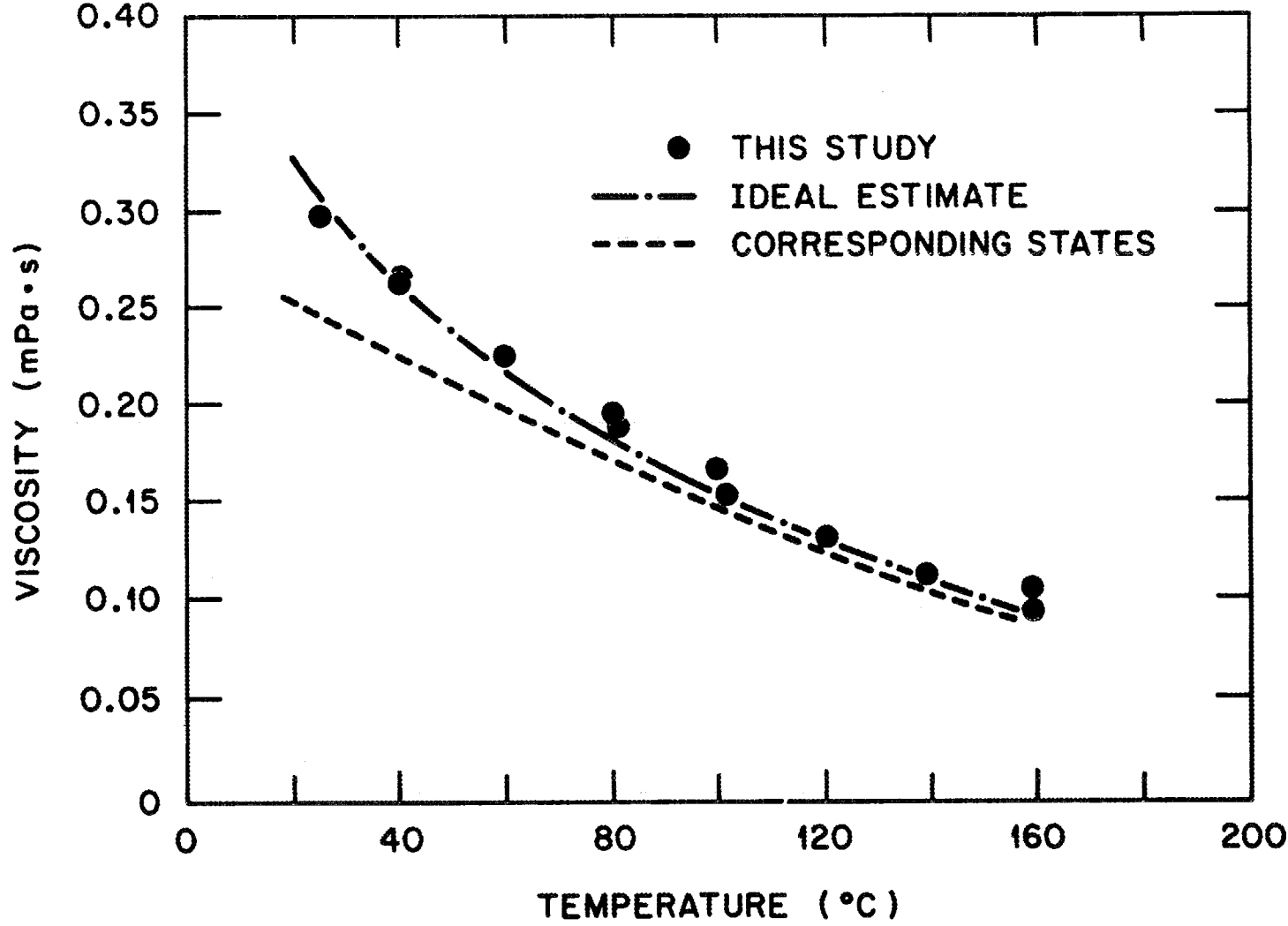


Fig. 17. Viscosity data and predictions for n-pentane/n-heptane binary (50-50 mol %).

high-temperature region. An interaction coefficient of unity was assumed. Note that the corresponding-states predictions involve no viscosity data or fitted parameters for pure components.

Interaction between hexane and isopropanol manifests itself as a significant depression of the mixture viscosity with respect to ideal behavior predictions (Fig. 18). This behavior results from a positive deviation from ideality, where the intermolecular forces between like molecules are much greater than those between unlike species. Consider the simple concept that the resistance to flow on a molecular level increases as the attraction between adjacent molecules increases. Essentially, the net effect of intermolecular attraction is diminished by mixing these two compounds. The converse of this example also seems to be valid. A negative deviation from ideality would show up as a significant increase in the viscosity of the mixture with respect to ideal behavior. A chloroform-acetone system was selected for demonstration of this effect. Unfortunately, the samples for light-scattering measurements were not sufficiently stable to permit analysis. Capillary viscometer measurements (0.47 mPa·s) did exhibit a 15% increase over the ideal predicted value (0.41 mPa·s) for a 50/50 mol. % mixture of chloroform and acetone at 25°C.

Both predictions for the hexane-isopropanol system were based on the same literature data. Corresponding-states values for the pure components were not used since isopropanol is a poor candidate for this type of estimation. As in the pentane-heptane case, the corresponding-states model ($\phi = 1$) and the Kendall equation merge as the temperature increases (Fig. 18). Also, the effect of interaction decreases as the temperature increases.

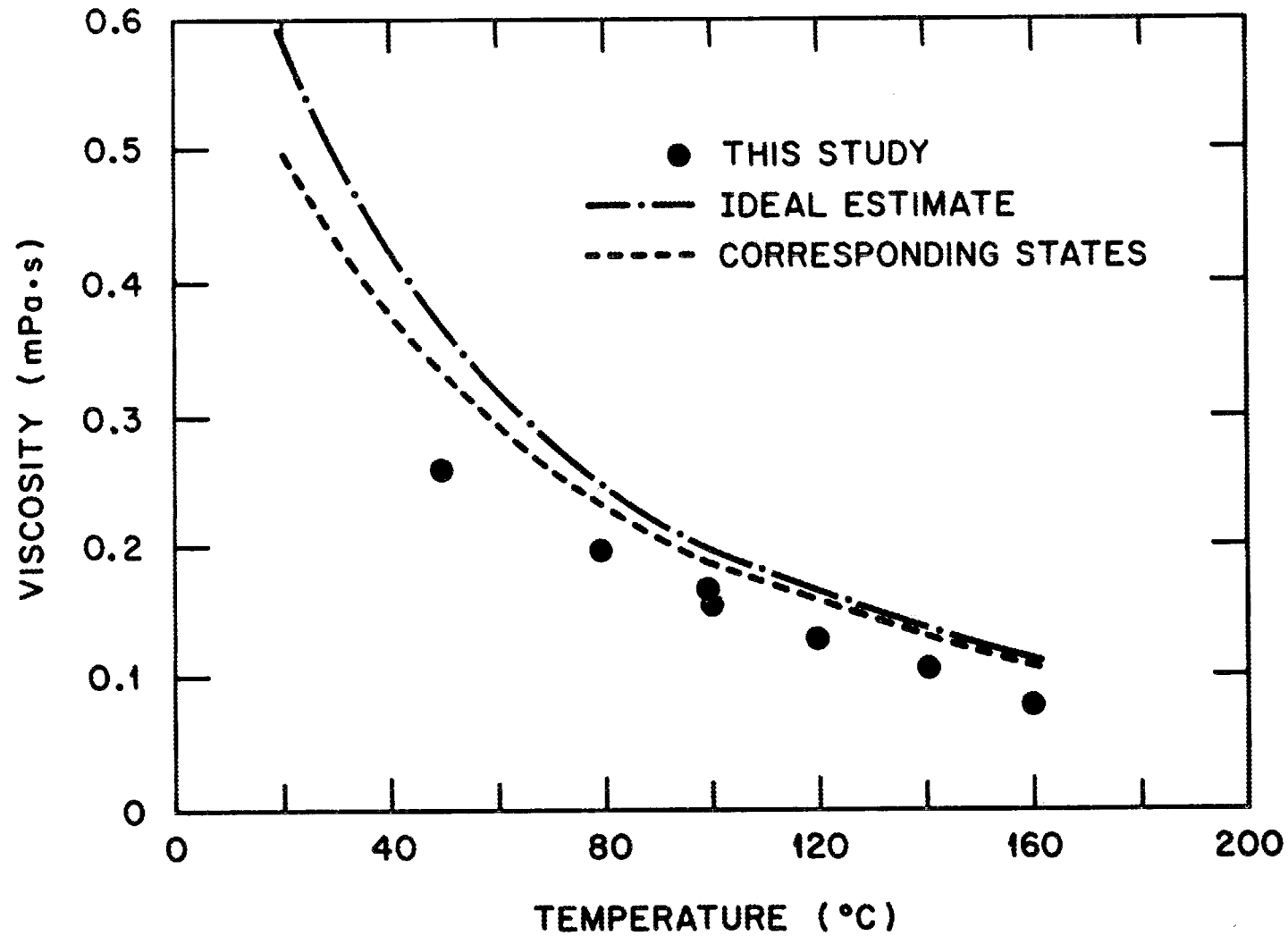


Fig. 18. Viscosity data and predictions for nonideal binary system (75.7 mol % n-hexane/24.3 mol % isopropanol).

IV. CONCLUSIONS

Dynamic light scattering from stabilized microparticles has been demonstrated to be an effective method for determining high-temperature liquid viscosities. It is essential that these submicron seed particles be physically and chemically inert, relatively monodisperse, and stabilized to prevent aggregation. In nonpolar media, stabilization can be achieved by providing a steric barrier that inhibits particle contact. The most effective barriers involve chemically binding suitable polymers to the particle surface so that they become organophilic. The suitability of the stabilizer is determined by the solubility properties of the polymer-solvent system. Stabilizers should readily dissolve in the suspending media.

The silica-stearyl alcohol microparticle preparation used in this study meets the criteria for use with a number of cyclic and aliphatic compounds. Measurements were made on n-pentane, n-heptane, cyclohexane, toluene, chloroform, and two model binary systems at temperatures ranging up to 90% of the critical temperature ($0.9 T_c$). Repeatability was generally >99%, and accuracy was estimated to be >98%.

The experimental results are in good agreement ($\pm 2\%$) with the best available literature values. High-temperature viscosities ($T_r > 0.7$) are best correlated by the three-parameter corresponding-states method of Letsou and Stiel. The average error of estimate of this correlation was 5%.

The two model binary systems that were investigated demonstrate the typical behavior of ideal and nonideal (interacting) mixtures. The viscosity of an ideal mixture (e.g., pentane-heptane) is accurately

characterized by the Kendall correlation. An interacting mixture (e.g., hexane--isopropanol) deviates from the ideal prediction in a manner that reflects the intermolecular forces between the species. In the high-temperature region ($T_r > 0.8$), the behavior of both types of systems is predicted by the corresponding-states method suggested by Teja and Rice.

In principle, this technique can be applied to any optically transparent fluid. It must be recognized that the stability of the microparticle seed imposes the most severe experimental limitation. While selection of a stabilizer is generally not obvious, the criteria for evaluation are well established and provide adequate guidance. Once the proper stabilizer chemistry has been established, relatively few complications should be expected.

LIST OF REFERENCES

LIST OF REFERENCES

1. N. J. Weinstein, "Fundamental Data Needs for Coal Conversion Technology," revised edition, RECON Systems, Inc., NTIS No. TID-28152, January 1981.
2. D. W. Brinkman, ed., "Design Properties of Coal Liquids: Edited Workshop Proceedings," U.S. DOE CONF-810381, Workshop held March 2-4, 1981, Fountainhead Lodge, OK (August 1981).
3. J. R. Van Wazer et al., Viscosity and Flow Measurement, Wiley-Interscience, New York, 1963.
4. K. B. Lyons et al., "Light Scattering Investigation of Brownian Motion in a Critical Mixture," Phys. Rev. Lett. 30(2), 42 (January 1973).
5. C. M. Sorenson et al., "Brownian-Diffusion Viscosity Measurement in a Thermal Gradient," Phys. Rev. Lett. 34(18), 1194 (May 1975).
6. B. J. Berne and R. Pecora, Dynamic Light Scattering, Wiley, New York, 1976.
7. B. Dahneke, ed., Measurement of Suspended Particles by Quasi-Elastic Light Scattering, Wiley, New York, 1983.
8. S. G. Brush, "Theories of Liquid Viscosity," Chem. Rev. 62, 513 (1962).
9. Huen Lee, "Transport Properties of Pure Fluids in the Dense Gaseous and Liquid States Including the Critical Point Region," Ph.D. dissertation, Northwestern University, Evanston, Ill., 1983.
10. J. H. Hildebrand, Viscosity and Diffusivity: A Predictive Treatment, Wiley-Interscience, New York, 1977.
11. J. O. Hirschfelder et al., Molecular Theory of Gases and Liquids, Chaps 4, 9, and 10, Wiley, New York, 1954.
12. K. S. Pitzer, "Corresponding States for Perfect Liquids," J. Chem. Phys. 7, 583 (1939).
13. H. Mori, "Statistical Mechanical Theory of Transport in Fluids," Phys. Rev. 112(6), 1829-62 (1958).
14. E. Helfland and S. A. Rice, "Principle of Corresponding States for Transport Properties," J. Chem. Phys. 32(6), 1642-44 (1960).
15. S. A. Rice and J. G. Kirkwood, "On an Approximate Theory of Transport in Dense Media," J. Chem. Phys. 31(4), 901-8 (1959).

16. K. S. Pitzer et al., "The Volumetric and Thermodynamic Properties of Fluids," J. Am. Chem. Soc. 77(13), 3427-40 (1955).
17. A. Letsou and L. I. Stiel, "Viscosity of Non-Polar Liquids at Elevated Pressures," AIChE J. 19(2), 409 (March 1973).
18. Reid et al., The Properties of Gases and Liquids, Chap. 9, McGraw-Hill, New York, 1977.
19. A. S. Teja and P. Rice, "Generalized Corresponding States Method for the Viscosities of Liquid Mixtures," Ind. Eng. Chem. Fundam. 20 77-81 (1984).
20. J. Kendall and K. P. Monroe, "The Viscosity-Composition Curve for Ideal Liquid Mixtures," J. Am. Chem. Soc. 39, 1787 (1917).
21. American Petroleum Institute, Division of Refining, Technical Data Book - Petroleum Refining, Chap. 11, New York, 1966.
22. C. Tsonopoulos et al., "Density, Viscosity, and Surface Tension of Coal Liquids at High Temperatures and Pressures," paper presented at 88th National AIChE Meeting, June 1980.
23. Grant Wilson et al., "Volatility of Coal Liquids at High Temperatures and Pressures," Ind. Eng. Chem. Process Des. Dev. 20, 94 (1981).
24. K. E. Starling et al., Development of a Thermodynamic Properties Correlation Framework for the Coal Conversion Industry - Phase II, DOE Report No. DOE/PC/30249-T3, March 1982.
25. S. Chandrasekhar, "Stochastic Problems in Physics and Astronomy," Rev. Mod. Phys. 15(1), 1-89 (1943).
26. B. Crosignoni et al., Statistical Properties of Scattered Light, Academic Press, New York, 1975.
27. A. Einstein, Ann. d. Phys. 17, 549 (1906).
28. B. Chu, Laser Light Scattering, Academic Press, New York, 1974.
29. J. C. Brown and P. N. Pusey, "Photon Correlation Study of Polydisperse Samples in Cyclohexane," J. Chem. Phys. 62(3), 1136-44 (February 1975).
30. C. B. Barger, "Measurement of a Continuous Distribution of Spherical Particles by Intensity Correlation Spectroscopy: Analysis by Cumulants," J. Chem. Phys. 61(5), 2134-38 (September 1974).
31. D. E. Koppel, "Analysis of Macromolecular Polydispersity in Intensity Correlation Spectroscopy. The Method of Cumulants," J. Chem. Phys. 57(11), 4184-4820 (December 1972).

32. H. Saad and Esin Gulari, "Diffusion of Carbon Dioxide in Heptane," J. Phys. Chem. 88(1) 136-39 (1984).
33. E. Matijevic, "Monodispersed Metal (Hydrous) Oxides - A Fascinating Field of Colloid Science," Acc. Chem. Res. 14, 22-29 (1981).
34. E. Matijevic, "Preparation and Characterization of Monodispersed Metal Hydrous Oxide Sols," Prog. Colloid Polym. Sci. 61, 24-35 (1976).
35. K. E. J. Barrett, ed., Dispersion Polymerization in Organic Media, Wiley, New York, 1974.
36. H. Sonntag and K. Strange, Coagulation and Stability in Disperse Systems, Halsted Press, New York, 1972.
37. G. E. Molau and E. H. Richardson, "Dispersion of Solid Particles in Organic Media," in Multicomponent Polymer Systems, Adv. Chem. Ser. (ACS) 99, 379 (1971).
38. J. M. Prausnitz, Molecular Thermodynamics of Fluid Phase Equilibria, Prentice-Hall, Inc., New York, 1969.
39. E. Jakeman, "Theory of Optical Spectroscopy by Digital Autocorrelation of Photon Counting Fluctuations," J. Phys. 3, 201-15 (1970).
40. A. K. Van Helden et al., "Preparation and Characterization of Spherical Monodisperse Silica Dispersions in Nonaqueous Solvents," J. Colloid Interface Sci. 81(2), 354-68 (June 1981).
41. Werner Stober et al., "Controlled Growth of Monodisperse Silica Spheres in the Micron Size Range," J. Colloid Interface Sci. 26, 62-69 (1968).
42. R. K. Iler, U.S. Patent 2,801,185.
43. V. Degiorgio and J. B. Lastokova, "Intensity Correlation Spectroscopy," Phys. Rev. A 4(5), 2033-50 (November 1971).
44. W. J. Lyman et al., Handbook of Chemical Property Estimation Methods, Chap. 26, McGraw-Hill, New York, 1977.
45. A. L. Lee and R. T. Ellington, "Viscosity of n-Pentane," J. Chem. Eng. Data 10(2), 306 (1965).
46. R. M. Hubbard and G. Brown, "Viscosity of n-Pentane," Ind. Eng. Chem. 35(12), 1276-80 (1943).
47. L. F. Albright and J. Lohrenz, "Viscosity of Liquids," AIChE J. 2(3), 290-95 (1956).
48. N. B. Vargaftik, Tables on the Thermophysical Properties of Liquids and Gases, Wiley, New York, 1975.

49. D. F. Williams, C. H. Byers, and C. H. Young, Viscosities of Polyaromatic Hydrocarbons: Experiment and Prediction, ORNL/TM-9410 (1985).
50. V. Degiorgio, ed., Light Scattering in Liquids and Macromolecular Solutions, Plenum Press, New York, 1979.
51. E. Rorris, M.S. Thesis, Department of Chemical Engineering, Northwestern University, Evanston, Ill. (1979).
52. C. F. Spencer and R. P. Danner, "Improved Rackett Equation for Prediction of Saturated Liquid Density," J. Chem. Eng. Data 17(2) 236-41 (1972).

APPENDIXES

Appendix A

TABULATION OF EXPERIMENTAL DATA
DETERMINED BY LIGHT SCATTERING

NOTE:

1. Units of viscosity = cP = centipoise = mPa•s
2. % CV = coefficient of variation for set of runs (#RUNS)
= (std. deviation/mean) × 100

FLUID= N- PENTANE

# RUNS	SAMPLE ID	TEMP. (C)	VISCOSITY (CP)	%CV
5	3.141	27.5	0.2206	0.45
5	3.141	35.0	0.2064	0.56
5	3.146	40.4	0.1986	0.57
5	3.141	44.2	0.1920	0.62
5	3.146	50.6	0.1824	0.42
5	3.146	60.2	0.1692	0.89
3	3.141	60.8	0.1691	0.52
5	3.146	61.1	0.1691	0.56
5	3.146	70.6	0.1566	1.03
5	3.146	70.7	0.1565	0.76
5	3.146	80.5	0.1440	0.18
5	3.146	81.2	0.1452	0.34
5	3.146	81.3	0.1453	1.37
5	3.146	90.4	0.1346	0.32
5	3.146	90.7	0.1348	1.35
5	3.146	100.7	0.1247	0.76

FLUID= N-HEPTANE

# RUNS	SAMPLE ID	TEMP. (C)	VISCOSITY (CP)	%CV
5	3.149	20.7	0.4233	1.91
5	3.149	20.8	0.4224	1.31
5	3.149	25.4	0.4012	0.55
5	3.148	50.1	0.3088	0.82
5	3.148	50.1	0.3088	0.73
5	3.149	72.5	0.2570	1.18
5	3.148	74.6	0.2476	1.34
5	3.148	75.0	0.2489	0.40
5	3.149	100.0	0.2012	0.67
5	3.148	102.3	0.1929	0.49
5	3.149	124.7	0.1625	0.90
5	3.148	126.3	0.1618	0.45
5	3.148	148.1	0.1318	0.18
5	3.148	148.2	0.1330	0.62
5	3.149	148.8	0.1282	1.03
5	3.150	163.3	0.1222	0.70
5	3.150	163.3	0.1162	3.00

FLUID= CYCLOHEXANE

# RUNS	SAMPLE ID	TEMP. (C)	VISCOSITY (CP)	%CV
5	3.097	21.8	0.9381	0.91
5	3.154	39.5	0.7151	0.68
5	3.154	39.7	0.7124	1.87
4	3.097	52.4	0.5843	0.89
5	3.154	58.2	0.5487	0.48
5	3.154	58.4	0.5563	1.07
4	3.154	77.2	0.4441	1.29
5	3.154	77.2	0.4430	0.85
5	3.097	101.0	0.3180	1.62
5	3.097	103.0	0.3178	0.40
5	3.154	105.0	0.3095	1.01
5	3.154	105.0	0.3116	1.04
5	3.154	120.0	0.2666	0.92
5	3.154	120.2	0.2650	0.49
5	3.154	140.0	0.2190	0.91
5	3.097	150.0	0.1949	0.15
5	3.154	160.4	0.1794	0.51
5	3.154	160.5	0.1807	0.35
5	3.154	179.6	0.1585	1.29
5	3.097	201.0	0.0968	0.92

FLUID= TOLUENE

# RUNS	SAMPLE ID	TEMP. (C)	VISCOSITY (CP)	%CV
5	3.153	38.8	0.4795	0.73
5	3.153	38.8	0.4727	0.94
5	3.111	50.0	0.4159	0.79
5	3.087	51.5	0.4140	0.84
5	3.153	58.9	0.3940	0.95
5	3.153	59.5	0.3922	0.85
5	3.153	80.4	0.3231	0.97
5	3.153	80.5	0.3257	1.51
5	3.111	100.5	0.2675	0.62
5	3.111	100.7	0.2678	1.01
5	3.087	101.5	0.2716	0.54
5	3.085	103.0	0.2728	0.96
5	3.153	105.2	0.2635	0.65
5	3.153	105.4	0.2628	0.43
5	3.153	122.1	0.2349	1.08
5	3.153	122.1	0.2352	1.30
5	3.153	140.0	0.2146	0.83
5	3.153	140.7	0.2131	0.79
5	3.087	150.0	0.2012	0.68
5	3.085	150.5	0.2145	0.86
5	3.111	151.7	0.1882	0.91
5	3.087	199.5	0.1294	0.22
5	3.085	200.5	0.1432	1.57
5	3.111	206.5	0.1186	0.90

FLUID= CHLOROFORM

# RUNS	SAMPLE ID	TEMP. (C)	VISCOSITY (CP)	%CV
5	3.112	54.0	0.4086	1.14
5	3.112	100.0	0.2821	0.56
5	3.112	102.0	0.2875	0.53
5	3.112	151.0	0.2001	0.32
5	3.112	202.0	0.1332	0.43

FLUID= 50% N-PENTANE / 50% N-HEPTANE

# RUNS	SAMPLE ID	TEMP. (C)	VISCOSITY (CP)	%CV
5	3.152	25.1	0.2976	0.43
5	3.152	39.7	0.2637	1.16
5	3.152	39.8	0.2637	0.94
4	3.152	40.0	0.2667	0.68
5	3.152	59.3	0.2263	0.88
5	3.152	59.9	0.2258	0.74
5	3.152	60.1	0.2258	1.00
5	3.152	79.7	0.1951	1.40
5	3.152	80.0	0.1968	0.35
5	3.152	80.7	0.1891	0.69
5	3.152	99.4	0.1674	0.54
5	3.152	99.7	0.1679	0.65
5	3.152	101.3	0.1547	0.40
5	3.152	101.5	0.1529	0.50
5	3.152	120.0	0.1326	0.90
5	3.152	120.0	0.1329	0.75
5	3.152	139.0	0.1136	0.88
5	3.152	139.0	0.1143	0.56
5	3.152	159.0	0.1070	3.60
5	3.152	159.0	0.0963	2.55

FLUID= 75% N-HEXANE / 25% ISOPROPANOL

# RUNS	SAMPLE ID	TEMP. (C)	VISCOSITY (CP)	%CV
5	3.165	49.6	0.2607	0.68
5	3.165	49.7	0.2595	0.55
5	3.165	50.0	0.2592	0.88
5	3.165	79.0	0.1964	1.03
5	3.165	79.4	0.1961	0.90
5	3.165	99.0	0.1662	0.37
5	3.165	99.5	0.1539	0.78
5	3.165	100.0	0.1531	1.33
5	3.165	119.5	0.1277	0.56
5	3.165	140.2	0.1061	0.95
5	3.165	159.5	0.0782	1.59
5	3.165	159.5	0.0785	1.37

Appendix B

VISCOSITY ESTIMATION METHOD OF LEE

The final form of Lee's correlation [Eq. (10)] is:

$$(\eta - \eta^*) \cdot \gamma \cdot 10^5 = \exp(2.933 g^a + 4.542 g^b) - 1 ,$$

where

$$a = 8.336 ,$$

$$b = 0.9228 ,$$

η = saturated-liquid viscosity, and

η^* = corresponding dilute-gas viscosity.

The coefficients of this equation were determined as the best estimates from a nonlinear regression analysis of $(\eta - \eta^*)\gamma$ vs g using argon data. Values of ϵ were also optimized ("fitted") in this procedure. The variables γ and g are defined as:

$$\gamma = (V_{1t})^{2/3} / \sqrt{M \cdot T_t} ,$$

$$g = X / (0.976\epsilon)^c ; \quad c = 2.3566 / X^{0.6673} ,$$

$$X = d / (T/T_t)^e ; \quad e = 0.07d^{2.73} ,$$

$$d = V_{1t} / V ,$$

where

V_{1t} = liquid molar volume at the triple point,

$\epsilon = V_{st} / V_{1t}$ = ratio of solid to liquid molar volume at the triple point,

M = molecular weight, and

subscript t refers to triple-point properties.

Lee has essentially changed his reference from the critical point to the triple point. The form of the equation was arrived at by invoking dimensionless analysis arguments and Andrade's hypothesis about the frequency of molecular vibration at the melting point. The expression for the dilute-gas viscosity was derived from the work of Rorris:⁵¹

$$\eta^* \cdot B \cdot 10^5 = 0.576 T_r^{0.41} - 35.5/\exp(10/\sqrt{T_r}) ,$$

and

$$B = V_c^{1/6} / \sqrt{M \cdot P_c} .$$

Fitted values of ϵ are available only for the limited set of substances considered by Lee. It is claimed that very few accurate measurements of the solid molar volume at the triple point exist. Therefore, the following estimation procedure for ϵ is recommended:

1. Estimate V_{1t} by extrapolation of a reliable liquid density correlation (i.e., Rackett⁵²) to the triple point or use literature data.
2. Use Lee's relation between V_{st} and the van der Waals co-volume parameter, b ,

$$P + \frac{a}{V^n} (V - b) = RT$$

(modified van der Waals equation of state),

at the critical point:

$$b = [(n - 1)/(n + 1)]V_c \text{ and } n = 2Z_c + \sqrt{4Z_c^2 + 1} .$$

Lee suggests: $V_{st} = 1.20 \cdot b$.

Appendix C

ESTIMATION OF REFRACTIVE INDEX

For a structureless liquid, the refractive index is a simple function of the specific volume (i.e., Lorenz-Lorentz relation). This follows from the fact that the molecular polarizability is essentially constant. Real fluids are not truly structureless, and empirical expressions correlate refractive index behavior most accurately. Eykman's equation is recognized as the most accurate method for predicting fluid refractive index as a function of temperature:

$$\frac{(n^2 - 1)}{(n^2 + 0.4)} \cdot V = R, \quad (\text{Eykman equation})$$

where

n = refractive index of fluid,

V = molar volume of fluid, and

R = constant = specific refraction (evaluated at standard conditions).

Solving for n yields

$$n = \frac{R + \sqrt{R^2 + 4 \cdot V(V + 0.4R)}}{2V}.$$

The application of this equation to fluids at temperatures above the normal boiling point has not been documented. However, recent data on liquid nitrogen [V. V. Alekseev et al., *Thermal Engineering (USSR)* 30(11), 1983; (p. 671, English tr.)] provide an opportunity to test the Eykman equation in the region between the boiling point and the critical point. The following table refers to measurements on saturated $N_2(\lambda)$:

Measurements on saturated $N_2(l)$

Temperature (K)	Refractive index value		Eykmann prediction	$\Delta\%$
	Measured	Literature		
85 (std)	0.6735	1.18846	—	—
90	0.713	1.18216	1.18271	0.0074
100	0.792	1.1683	1.16866	0.014
120	0.951	1.12886	1.12763	0.162
Avg. deviation = 0.061%				

There are a large number of accurate correlations ($\pm 0.5\%$) for the density of a saturated liquid. We have employed the modified Rackett equation in this study.⁵¹ The refractive index of the mixture was obtained by taking a simple mol average of the pure component values. These average values were checked at room temperature and were found to be accurate.

Appendix D

COMPUTER PROGRAM DOCUMENTATION

Program LSD.ST1 (listing attached) was used to automate the light-scattering measurements. The program was written in Applesoft Basic for use on an Apple IIe computer to interface with a Langley Ford 1096 (LF 1096) Autocorrelator. A computer clock was used to date files and to tag each run with an identifying time.

The organization of the program is as follows:

1. Initialization -- set up raw data files (D) and calculated results files (C).
2. Specify experimental parameters: laser wavelength, sample temperature, refractive index, standard particle size, and estimated viscosity.
3. Select run parameters -- number of runs, and run time.
4. Set up Apple IIe and LF1096 for data logging.
5. Data logging of sequential light-scattering runs:
 - a. Apple IIe accepts 17 LF1096 identifiers.
 - b. Apple IIe accepts autocorrelation channel data.
 - c. Quadratic least-squares calculation is performed using channel data.
 - d. Raw data and calculated results are stored on magnetic disk.Steps a through d are repeated for the number of runs selected.
 - e. Options are to return to steps 2 or 3 or to exit the program.

The quadratic regression program (LSD.ST1) uses the same algorithm that is used in the Langley Ford model ANO1 Analysis Program. Both programs yield the same results. The use of our own program allowed us to control operation and log data much more easily.

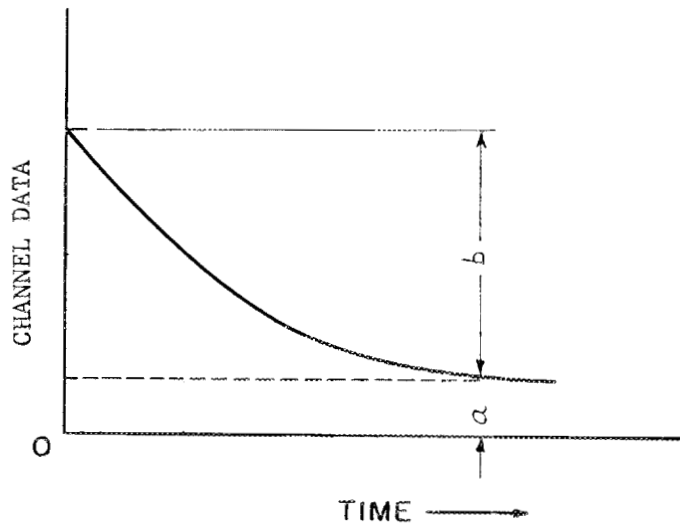
The only unusual aspect of the calculations was the use of a weighted analysis. A weighted analysis is needed because of the nature of the detector (PMT) and the transformation of the data. The PMT is a square-law detector. The uncertainty in the measurement (number of counts = N) is proportional to \sqrt{N} . This needs to be taken into account during the regression by weighing each data point.

According to Eq. (34b), we can write:

$${}^2A^*(t) = a + b[A^*(t)]^2 \quad a, b \text{ constants ,}$$

$$\text{and } {}^2A^*(t) = \text{autocorrelation channel data} \\ = \text{CD .}$$

We can picture this as:



To apply the cumulant analysis, we transform our data (CD) to Y as:

$$Y = CD - a .$$

In practice, the factor a (base line) is accurately estimated by obtaining channel data at large values of t. The actual ordinate in the analysis is:

$$Y' = \ln Y = \ln (CD - a) .$$

The standard deviation of the transformed variable, Y', is:

$$\sigma_{i'} = \frac{d}{dY} (Y') \cdot \sigma_i = \frac{d}{dY} (\ln Y) \cdot \sigma_i ,$$

where σ_i is the standard deviation of Y.

It is generally assumed that the channel data have the same statistics as a PMT count. Therefore,

$$\sigma_i = \sqrt{CD} ,$$

and

$$\sigma_{i'} = \frac{\sqrt{CD}}{CD - a} .$$

Basic Data Logging Program - LSD.ST1

```

17 REM
18 REM DECLARATION STATEMENTS
19 REM
20 LOMEM: 16384
30 DIM G(400),A(30),B(30)
40 TEXT : HOME
45 PRINT "DATA STORAGE PROGRAM": PRINT
50 X = FRE (0):D$ = CHR$ (4):I$ = CHR$ (9)
51 G$ = CHR$ (13):E$ = G$ + D$:V$ = ".1"
52 PRINT D$;"PR#5": PRINT D$"IN#5"
53 INPUT " ";T$
54 U$ = LEFT$ (T$,2) + MID$ (T$,4,2)
55 PRINT D$"PR#0": PRINT D$"IN#0"
56 PRINT "? OPTIONAL FILENAME IDENTIFIER(Y:N)?": INPUT L$
57 IF L$ = "N" GOTO 59
58 PRINT "ENTER FILE ID SUFFIX": INPUT V$:V$ = "." + V$
59 A$ = "D" + U$ + V$:B$ = "C" + U$ + V$
62 REM
63 REM SET-UP DATA&CALC FILES
64 REM
66 PRINT D$;"OPEN";A$;","D2": PRINT D$;"CLOSE";A$
67 PRINT D$;"OPEN";B$;": PRINT D$;"CLOSE";B$
68 TEXT : HOME
69 REM
70 REM SPECIFY EXP. PARAMTERS
71 REM
72 PRINT D$;"PR#4": PRINT I$;"1D": PRINT I$;"3P": PRINT
D$;"PR#0"
75 PRINT "SET EXP. PARAMETERS"
80 PRINT "INPUT LASER WAVELENGTH(NM)": INPUT WL:A(22) =
WL:B(12) = WL
90 PRINT "INPUT SAMPLE TEMP.(C)": INPUT T:A(21) = T:B(11)
= T
100 PRINT "INPUT REF. INDEX": INPUT RI:A(23) = RI:B(13) =
RI
110 PRINT "INPUT PARTICLE SIZE(MICRONS)": INPUT DP:A(24) =
DP:B(14) = DP
120 PRINT "INPUT VISCOSITY EST.(CP)": INPUT VISC:A(25) =
VISC:B(15) = VISC
124 REM

```

LSD.ST1

```

125 REM   SELECT RUN PARAMETERS
126 REM
129 PRINT : PRINT
130 PRINT "SELECT AUTO-RUN PARAMETERS"
135 PRINT "SET 1096 TO RS-232 CONTROL": PRINT : PRINT
136 PRINT "PRESS(I/O;ENTER;2;ENTER) ON 1096"
137 PRINT "PRESS RESET&ANALYZE": PRINT : PRINT
140 PRINT "INPUT #RUNS DESIRED": INPUT NR:J1 = 1:A(20) =
NR:B(10) = NR
150 PRINT "INPUT RUN TIME(SEC)": INPUT RT:A(19) = RT:B(9)
= RT
152 X = NR: GOSUB 4000:N1 = X1:N2 = X2:N3 = X3
154 X = RT: GOSUB 4000:R1 = X1:R2 = X2:R3 = X3
159 REM   ***SETUP SSC TO INTERFACE
W/1096*****
160 PRINT D$;"PR#4": PRINT CHR$(9);"M E": PRINT I$;"ID":
PRINT I$;"3P": PRINT D$;"IN#4"
161 REM
162 REM   COMPUTER CTRL OF 1096
163 REM
164 PRINT "K";: GOSUB 3000: PRINT "U";: GOSUB 3000: PRINT
4;: GOSUB 3000: PRINT G$;: GOSUB 3000: PRINT 1;: GOSUB
3000: PRINT G$;: GOSUB 3000: PRINT "M";: GOSUB 3000: PRINT
G$;
165 GOSUB 3000: PRINT R1;: GOSUB 3000: PRINT R2;: GOSUB
3000: PRINT R3;: GOSUB 3000: PRINT G$;: GOSUB 3000: PRINT
4;: GOSUB 3000: PRINT G$;: GOSUB 3000: PRINT N1;: GOSUB
3000: PRINT N2;
166 GOSUB 3000: PRINT N3;
167 GOSUB 3000: PRINT G$;: GOSUB 3000: PRINT "R";: GOSUB
3000: PRINT "O";: GOSUB 3000: PRINT G$;: GOSUB 3000: PRINT
1;: GOSUB 3000: PRINT G$;: GOSUB 3000
175 REM
176 REM   DATA-LOGGING ROUTINE(1096-APPLE)
177 REM       1. ACCEPT 17 RUN ID'S
178 REM
210 GOSUB 1005:A(1) = X
240 FOR I = 2 TO 17: GOSUB 1000
250 A(I) = X: NEXT I
260 BKS = A(10):NC = BKS * 76
264 REM
265 REM       2. ACCEPT CHANNEL DATA
266 REM
270 FOR I = 1 TO NC: GOSUB 1000
280 G(I) = X: NEXT I
290 PRINT D$;"PR#0"
292 PRINT D$;"IN#0": REM   ***END DATA LOGGING***

```

LSD.ST1

```

293 PRINT D$;"PR#5": PRINT D$"IN#5"
294 INPUT "#";MO,DW,DT,HR,MN,SEC
295 PRINT D$;"PR#0": PRINT D$"IN#0"
296 B(23) = HR + (MN + SEC / 60.) / 60.
302 K$ = U$ + "." + STR$(A(1)): REM ***DEFINE RUN ID
=DATE.RUN# ***
303 S = A(8):QR = S / 100:QI = INT(QR)
304 A(8) = (QI + INT(10 * (QR - QI)) / 10) * 10 ^ ((INT
(S / 10) - S / 10) * 10)
305 S = A(8)
307 REM
308 REM STORE RAW DATA IN FILE
309 REM
310 PRINT D$;"APPEND";A$
320 PRINT D$;"WRITE";A$
321 PRINT K$
340 FOR I = 1 TO 17
350 PRINT A(I): NEXT I
360 FOR I = 19 TO 25: PRINT A(I): NEXT I
370 FOR I = 1 TO NC
380 PRINT G(I): NEXT I
385 PRINT D$;"CLOSE";A$
390 GOSUB 1500: REM ***PERFORM ONLINE CALCULATIONS***
400 IF J1 = NR GOTO 420
405 PRINT D$;"PR#4": PRINT CHR$(9);"M E": PRINT
D$;"IN#4"
410 J1 = J1 + 1: GOTO 210
420 PRINT "?NEW DATA-FILE?(Y:N)": INPUT E$
430 IF E$ = "Y" GOTO 60
460 PRINT "?NEW EXP. PARAMETERS?(Y:N)": INPUT F$
470 IF F$ = "Y" GOTO 70
480 PRINT "?NEW RUN PARAMETERS?(Y:N)": INPUT H$
490 IF H$ = "Y" GOTO 130
500 END
997 REM
998 REM 1096(PRINT)--->APPLE HANDSHAKE
999 REM
1000 PRINT ".";
1005 INPUT "";X
1010 RETURN
1500 REM
1501 REM REGRESSION ROUTINE(2ND ORDER)
1502 REM
1505 B(3) = A(3):B(4) = A(8):B(5) = A(9):B(6) = A(10):B(7)
= A(11):B(8) = A(14):B(16) = A(4):DS = 26
1510 N = (BKS - 1) * 76 + 65:L8 = 0:N1 = N + 7
1514 REM

```

LSD.ST1

```

1515  REM  CALC. BASELINE VALUES
1516  REM
1520  FOR I = N TO N1
1530  L8 = G(I) + L8: NEXT I
1540  L8 = L8 / 8:P2N = 0:TST = 0
1550  FOR I = 1 TO BKS
1560  P2N = P2N + G(76 * (I - 1) + 74) * G(76 * (I - 1) +
75)
1570  TST = TST + G(76 * (I - 1) + 73): NEXT I
1580  P2N = P2N / TST
1590  RA = L8 / P2N:B(17) = RA
1600  REM
1601  REM : CALC. REGRESSION SUMS
1602  REM
1610  M = 0:S1 = 0:S2 = 0:S3 = 0:S4 = 0:S5 = 0:S6 = 0:S7 =
0:S0 = 0:CNU = 0
1611  LT8 = 20 * SQR (L8)
1620  FOR J = 0 TO BKS - 1
1630  FOR I = 1 TO 72 + 8 * (A(11) - 2)
1635  K = J * 76 + I:GD = G(K) - L8:WF = GD * GD / G(K)
1638  M = M + 1
1639  IF G(K) < LT8 GOTO 1678
1640  S0 = S0 + WF:S1 = S1 + M * WF:S2 = S2 + M * M * WF:S3
= S3 + M * M * M * WF:S4 = S4 + M ^ 4 * WF
1660  Y = LOG ( ABS (G(K) - L8))
1670  S5 = S5 + Y * WF:S6 = S6 + M * Y * WF:S7 = S7 + M * M
* Y * WF
1678  GOTO 1680
1679  CNU = CNU + 1
1680  NEXT I
1690  NEXT J
1695  CNU = M - CNU:M = S0:B(18) = CNU
1700  REM
1701  REM : CALC. REGRESSION COEFF.
1702  REM
1710  D = M * S2 * S4 + S1 * S3 * S2 * 2 - S2 ^ 3 - S3 * S3
* M - S4 * S1 * S1
1720  E = (S5 * S2 * S4 + S1 * S3 * S7 + S2 * S6 * S3 - S7 *
S2 * S2 - S3 * S3 * S5 - S4 * S6 * S1) / D
1730  B = (M * S6 * S4 + S5 * S3 * S2 + S2 * S1 * S7 - S2 *
S6 * S2 - S7 * S3 * M - S4 * S1 * S5) / D
1740  C = (M * S2 * S7 + S1 * S6 * S2 + S5 * S1 * S3 - S2 *
S2 * S5 - M * S3 * S6 - S7 * S1 * S1) / D
1750  BTA = EXP (E) / L8:B(19) = BTA
1760  GAMMA = - B / (2 * S)
1770  PLD = 4 * C / (B * B):B(20) = PLD
1780  CPD = 1.1566E + 5 * RI * RI * (T + 273.2) / (GAMMA *

```

LSD.ST1

```
VISC * WL * WL):B(21) = CPD
1790 CVISC = 1.1566E + 5 * RI * RI * (T + 273.2) / (GAMMA *
DP * WL * WL):B(22) = CVISC
1794 REM
1795 REM STORE RUN ID & CALC.VALUES IN "C" FILE
1796 REM
1800 PRINT D$;"APPEND";B$
1810 PRINT D$;"WRITE";B$
1820 PRINT K$: PRINT DS
1825 FOR I = 3 TO 26
1830 PRINT B(I): NEXT I
1840 PRINT D$;"CLOSE";B$
1850 RETURN
2994 REM
2995 REM APPLE(COMMAND)----->1096 HANDSHAKE
2996 REM
3000 GET X$
3011 RETURN
3994 REM
3995 REM CONVERSION OF X(3) TO SERIAL DIGITS(X1,X2,X3)
3996 REM
4000 X1 = INT (X / 100)
4002 X2 = INT ((X - 100 * X1) / 10)
4003 X3 = X - 100 * X1 - 10 * X2
4004 RETURN
```

INTERNAL DISTRIBUTION

1. J. M. Begovich
2. B. M. Benjamin
3. R. R. Brunson
- 4-8. C. H. Byers
9. H. D. Cochran
10. M. T. Harris
11. J. R. Hightower
12. D. D. Lee
13. F. R. Mynatt
14. B. R. Rodgers
15. C. D. Scott
16. J. S. Watson
17. R. M. Wham
18. R. G. Wymer
19. Central Research Library
20. Y-12 Technical Library, Document Reference Section
- 21-22. Laboratory Records
23. Laboratory Records, R.C.
24. ORNL Patent Section

EXTERNAL DISTRIBUTION

25. J. J. Perona, Department of Chemical Engineering, University of Tennessee, Knoxville, TN 37916
- 26-30. D. F. Williams, Department of Chemical Engineering, University of Washington, Seattle, WA 98105
31. M. C. Wittels, Office of Basic Energy Sciences, DOE, Mail Station J-325, GTN, Washington, D.C. 20545
32. I. L. Thomas, Office of Basic Energy Sciences, DOE, Mail Station J-321, GTN, Washington, D.C. 20545
33. Office of Assistant Manager for Energy Research and Development, U.S. Department of Energy -- ORO, Oak Ridge, TN 37831
- 34-60. Technical Information Center, Oak Ridge, TN 37830